

We would like to thank the referees for reviewing our manuscript and for their helpful comments and suggestions. Our point-by-point responses are given below. Page and line numbers given refer to the reviewed version of the manuscript. The original reviewer comments are typeset in **gray**, the replies in **black**, while the proposed changes in the text are in **blue**.

#### **Anonymous Referee #1**

1) My only concern with the manuscript, at present, is the detrimental effect of the current length and breadth of the present manuscript on the overall readability and, possibly, even limiting further discussion of both (1) the data collection and (2) the data comparison with global and regional models. The manuscript would appear to be well-suited for division into two companion manuscripts, with one containing the description and comparison of the instrumentation and observational data, and a second manuscript containing the measurement-model discussion.

We agree that in principle the scope and findings of the manuscript could be separated into two companion publications, and we discussed this when starting on the manuscript. However, we concluded that the combination of the new high resolution CH<sub>4</sub> isotope data with the data interpretation using models in one manuscript is in fact one of the strengths of our work, and we therefore decided to keep these two aspects together in order to increase the impact of the work.

2) It appears as though the TREX-QCLAS collected only half as many measurements as the IRMS system (Fig. 2). Is there cause for concern regarding reliability, despite a moderate increase in throughput? I commend the authors for their discussion of the inter-calibration and comparison of the two measurement techniques, both with regards to isotopic and mole fraction measurements.

Both analytical systems were newly developed and for the first time applied in an extended field campaign, and there are periods without data, indeed more so for the QCLAS system than for the IRMS system, which is partly due to the fact that high quality measurements with the QCLAS system started later. The authors are convinced that there is no fundamental cause for concern regarding the TREX-QCLAS system as demonstrated by a significantly improved performance by the end of the campaign as mentioned in the method section on page 10 Line 283 – 289. Similar instrumentation developed by the authors has been applied for extended field campaigns (e.g. Wolf et al. Biogeosciences, 2015). The fact that the TREX-QCLAS system started later and that various kind of instrument malfunctions led to a number of interruptions for both analytical systems is mentioned in the result section of the manuscript on page 14 Line 417 – 422.

Specific comments:

3) Line 89: This is a poor topic sentence for this paragraph. This paragraph should be re-structured.

The respective sentence was moved to page 4 Line 97, after the wording: ... and given in per mill (‰). CH<sub>4</sub> mole fractions ...

4) Line 163 and elsewhere: Manufacturers need additional location information (e.g. line 163, Varian, Inc.) and sufficient information is missing for some manufacturers (e.g. VICI, manufacturer of Valco valves).

The following information was added:

Line 163: ... by a Varian scroll pump (Agilent Technologies Inc., USA)

Line 178: ... Thermo Delta Plus XP for carbon isotopes, both Thermo Fisher Scientific Inc., Germany)

Line 187: ... using removable frits (CEF1F, Valco Instruments Company Inc., USA)

Line 189: ... with Valco fittings (ECEP211.0F, Valco Instruments Company Inc., USA).

Line 202: ... directed either Helium (He, BIP quality, Air Products and Chemicals Inc., USA) or ...

Line 204: ... by mass flow controllers (MFC, MKS Instruments Inc., USA).

Line 210: ... by a mini pump (P200-GAS-12V, Xavitech AB, Sweden).

Line 241: A custom made LabVIEW software program (National Instruments Corp., USA) was ...

5) Line 134: A summary of the contents of each section seems self-explanatory and does not add value to the manuscript.

The respective section was shortened to:

... and one QCLAS-instrument developed at Empa. The compatibility of both analytical techniques for CH<sub>4</sub> mole fractions,  $\delta^{13}\text{C-CH}_4$  and  $\delta\text{D-CH}_4$  is assessed and the obtained high-resolution isotope dataset is exploited using a novel moving Keeling plot method. Comparison of measurement results with calculations from two different models (TM5 and FLEXPART-COSMO) and two inventories (EDGAR, TNO-MACC) indicates the potential of this approach to better constrain on isotope source signatures and emissions in atmospheric models.

6) Lines 196-205: Are the valve abbreviations used for descriptive purposes or are they part numbers? If they are for descriptive purposes, it would be great if they also appeared in Fig. 1.

Figure 1 has been updated accordingly.

7) Line 191: the authors have described two traps, one for pre-concentration ("PreCon") and a second for focusing ("Focus"). Please replace "focus units" with "trapping units" or something similar.

The respective sentence was changed to:

The PreCon and Focus trapping units were glued together with a PT-100 temperature sensor in heat-conducting two component epoxy on a brass standoff.

8) Line 222: capitalize "plus"

The actual IRMS product names from Thermo Fisher do not use capitals: Delta plus XL or Delta plus XP

9) Line 232: In Fig. 1, the temperature for the PoraPLOT Q is listed as 0 °C, not 5°C. Please clarify.

The correct temperature is 5°C, this was updated in figure 1.

10) Lines 227-228 and 234: repeatability estimate needs +/-; is the estimate reported as SD or SE?

The  $\pm$  sign has been added and the estimate is reported as SD (also added).

11) Line 237: "base" should be "basis"

Done

12) Line 238: please define "target gas"

We have added the following sentence:

... was analyzed as a quality control tool in order to monitor the long term stability of the analytical technique.

13) Line 245-257: would units of  $\mu\text{mol/mol}$  not be better considering the magnitude of the concentration, as well and bringing uniformity to the units reported for the laser reference gases?

The authors prefer to keep the units for CH<sub>4</sub> mole fractions in the reference air cylinder in  $\text{nmol/mol}$ , which is a common unit for close to ambient CH<sub>4</sub> mole fractions and also used in Figures 2 – 5 and Figure 9.

14) Line 253: I think something is confused here. I believe the authors intend to report no significant linearity, however, as worded ("no non-linearity"), the opposite is conveyed. If there was significant linearity, please report the change in isotopic value with concentration.

This confusion arose from the somewhat unconventional use of the term "non-linearity" in isotope research. The sentence has been clarified as follows

The linear response of the analytical system (independence of the  $\delta$  value on the amount of CH<sub>4</sub> analyzed) was verified by injecting various volumes of reference air up to a volume equivalent to 2700 nmol/mol.

15) Line 276: A direct comparison of the throughput between systems would be helpful earlier in the manuscript. It is referenced later, but I was already wondering about the comparison at first presentation.

The authors agree and added the following sentence:

This translates into an analysis time of 54 minutes per sample of ambient or pressurized air.

16) Line 333: remove "see" in brackets.

Done

17) Lines 334-336: How were these source signatures "adjusted"? Please expand.

The sentence was misleading and has been modified as follows (see comment 10 from referee 2).

The emission inventory was built according to a double constraint: 1<sup>st</sup>, each source signature must be chosen within its own uncertainty interval, and 2<sup>nd</sup>, the resulting global average source signature must be compatible with the global source signature that is inferred from the observations (and that is known with a much better precision than the individual source signatures).

18) Line 358: "Denmark, and Poland"

Done.

19) Line 444: what might be instrumental causes of offsets between systems? Combustion/HTC versus spectroscopy? Further discussion here would be interesting.

For  $\delta^{13}\text{C}$ -CH<sub>4</sub> only a slight offset between TREX-QCLAS and IRMS results of  $0.05 \pm 0.03$  ‰ was observed. TREX-QCLAS results for  $\delta\text{D}$ -CH<sub>4</sub> during the Cabauw campaign were on average  $-3.6 \pm 0.4$  ‰ lower than values obtained by IRMS and discrepancies were most pronounced for low  $\delta\text{D}$ -CH<sub>4</sub> values. Differences for  $\delta\text{D}$ -CH<sub>4</sub> between both techniques are irrespective of the fact, that recently a link was established between the CH<sub>4</sub> isotopic composition and the international reference materials VPDB and VSMOW, in the framework of the INGOS project (Sperlich et al., 2016) and both laboratories already performed inter-laboratory measurements in a previous campaign as published by Eyer et al. (2016). The enhanced discrepancies for low  $\delta\text{D}$ -CH<sub>4</sub> values, might be explained by a non-linear response of one of the applied techniques. To present the above argumentation the following wording was added to page 16 Line 463:

... as indicated by the red dashed lines (WMO, 2014). Individual measurement pairs, however, can show significantly larger deviations for aforementioned reasons. Differences for  $\delta\text{D}$ -CH<sub>4</sub> between both techniques are higher than expected as both laboratories refer their measurements to MPI-BGC, who recently established a link between the CH<sub>4</sub> isotopic composition and the international reference materials VPDB and VSMOW, in the framework of the INGOS project (Sperlich et al., 2016). Therefore, remaining differences can only be rationalized by uncertainties in propagating the scale or by instrumental issues. The enhanced discrepancies for low  $\delta\text{D}$ -CH<sub>4</sub> values might originate from a non-linear response of one of the applied analytical techniques. The mean offset ...

20) Fig. 1. Labeling of valves and matching description in text would be helpful

Done. See also response on comment #6 of reviewer #1.

We would like to thank the referees for reviewing our manuscript and for their helpful comments and suggestions. Our point-by-point responses are given below. Page and line numbers given refer to the reviewed version of the manuscript. The original reviewer comments are typeset in **gray**, the replies in **black**, while the proposed changes in the text are in **blue**.

## Anonymous Referee #2

1) Bag samples from the Royal Holloway University of London laboratory are presented in Figure 2, but not referenced anywhere that I can find in the main text. I think these measurements should either be discussed in the body of the manuscript, or removed from Figure 2.

The IRMS data from RHUL were removed from Figure 2 in order to not further increase the complexity and length of the manuscript.

2) I don't know if this is a convention in the literature, but my understanding of the nomenclature used in this paper is that "isotopic signature" is used to describe the isotope ratio of the CH<sub>4</sub> emitted from a particular source, whereas "isotope source signature" or just "source signature" is used to describe the combined isotopic signature of the sources that might have contributed to a measured air mass. I found this a very confusing (e.g. see L378 - 380), and perhaps not the most descriptive set of terms. Perhaps I am confused, but I wonder whether the authors could come up with a naming system that describes these terms more clearly. Mainly, when I read the term "source signature" I think that it must refer to the delta value that is the property of a particular source. This does not seem to be its use in this paper.

The terms "isotopic signature" and "isotopic source signature" were used to describe both the isotopic composition of a "single process" CH<sub>4</sub> source and a "combined or mixed source", which may indeed lead to confusion. To resolve this, signatures of combined or mixed sources are now referred to as "mean isotopic signature" or "isotopic composition". To clarify the wording the following section on page 13 Line 383 – 391 was rephrased:

The isotopic composition of CH<sub>4</sub> emissions were estimated using the Keeling plot technique (Keeling, 1961; Pataki et al., 2003). This method allows determining the isotopic signature of a single source process or the mean isotopic signature of combined source processes that mix into a background reservoir from the observed ambient isotopic composition and mole fraction. An implicit assumption of the Keeling plot approach is that the isotopic composition and mole fraction of the background reservoir and the isotopic composition of the source or the combined source stay constant over the time range of the analysis. This may not always apply as the relative contribution of individual CH<sub>4</sub> sources or their isotopic signature may change over time.

In addition, the terms "isotopic source signature" and "isotopic signature" were replaced on

page 13 Line 379: "isotopic source signatures" replaced by "mean  $\delta^{13}\text{C}$  and  $\delta\text{D}$  isotopic signatures"

page 18 Line 526: "source signatures" replaced by "mean  $\delta\text{D}$  signature"

page 18 Line 549: "isotopic signature" replaced by "mean isotopic signatures"

page 18 Line 552: "isotopic signatures" replaced by "mean isotopic signatures"

page 18 Line 554: "isotopic signature" replaced by "mean isotopic signature"

page 19 Line 556: "cumulative source signature" replaced by "mean isotopic signature"

page 19 Line 560: "source signature" replaced by "mean isotopic signature"

page 19 Line 571: " $\delta^{13}\text{C}$  source signatures" replaced by "mean  $\delta^{13}\text{C}$  signatures"

page 19 Line 572: " $\delta\text{D}$  source signatures" replaced by "mean  $\delta^{13}\text{D}$  signatures"

page 19 Line 575: " $\delta^{13}\text{C}$  and  $\delta\text{D}$  source signatures" replaced by "mean  $\delta^{13}\text{C}$  and  $\delta\text{D}$  signatures"

page 19 Line 577: "source signatures" replaced by "mean isotopic signature"

page 19 Line 582: "isotopic source signatures" replaced by "mean isotopic signature"

page 20 Line 589: "isotope source signature" replaced by "mean isotopic signature"

page 20 Line 595: "source signature" replaced by "signature"

page 20 Line 595-596: "source signature" replaced by "signature"

page 20 Line 601: "source signatures" replaced by "[mean isotopic signatures](#)"  
 page 21 Line 621: "isotopic source signatures" replaced by "[isotopic composition](#)"  
 page 21 Line 624: "isotopic source signatures" replaced by "[mean isotopic signatures](#)"  
 page 21 Line 629: "isotopic source signature time series" replaced by "[time series for the mean isotopic signatures](#)"  
 page 21 Line 631: "source signatures" replaced by "[mean isotopic signatures](#)"  
 page 21 Line 633: "isotope source signatures" replaced by "[mean isotopic signatures](#)"  
 page 21 Line 635: "source signatures" replaced by "[mean isotopic signatures](#)"  
 page 21 Line 635-636: "source signatures" replaced by "[signatures](#)"  
 page 21 Line 637: "source signatures" replaced by "[mean isotopic signatures](#)"  
 page 21 Line 639: "CH<sub>4</sub> isotope source signature distributions" replaced by "[mean CH<sub>4</sub> isotopic signatures](#)"  
 page 21 Line 646: "source signatures" replaced by "[mean isotopic signature](#)"  
 page 22 Line 651: "isotope source signatures" replaced by "[mean isotopic signatures](#)"  
 page 22 Line 654: "source signatures" replaced by "[mean isotopic signatures](#)"  
 page 22 Line 665: "isotopic source signatures" replaced by "[mean isotopic signatures](#)"  
 page 22 Line 670: "source signatures" replaced by "[mean isotopic signatures](#)"  
 page 22 Line 677: "source signatures" replaced by "[mean isotopic signatures](#)"  
 page 22 Line 678: "source signatures" replaced by "[mean isotopic signatures](#)"  
 page 35 Line 798: "isotopic source signatures" replaced by "[mean isotopic signatures](#)"  
 Page 36 Line 809: "source signatures" replaced by "[mean isotopic signatures](#)"

Furthermore the title of section 4.2 was changed to:

[Isotope identification of the mean CH<sub>4</sub> source](#)

Specific comments:

3) L51: "representative of"

The wording "...at multiple sites that are representative for the entire European domain." seems to be appropriate.

4) L94: Shouldn't this be "Pee Dee Belemnite"?

Done

5) L159: What does "limited air conditioning mean"?

Wording preplaced by:

[Since this room is not commonly used as laboratory, it has an air-conditioning with limited cooling capacity and ...](#)

6) L162: Define "o.d" in this section.

Done

7) L271: "a lower offset in d13C of 1.58permil". I think this statement would benefit from spelling out a little more clearly. What was the offset before, and how has it changed?

The reasoning for the lower offset was already given in the text a few lines before. To clarify the issue and to add details on the offset during previous measurements the text on page 9 Line 268 ff was changed too:

Due to the lower heating power, the duration of the desorption step had to be extended, which led to an improved separation from residual bulk gases (e.g. N<sub>2</sub> and O<sub>2</sub>). Lowering the O<sub>2</sub> enhancement in the gas matrix is also the main reason for a lower offset in  $\delta^{13}\text{C}$  of 1.58 ‰, with respect to the MPI-scale, as compared to 2.3 ‰ in previously published results (Eyer et al., 2015).

8) L286 - 288: What adjustments were made? Can you provide general details?

The following information has been added on page 10 Line 286:

Additional adjustments in the preconcentration procedure and in the analytical routine for isotope analysis improved the repeatability to 0.18 ‰ and 0.85 ‰ for  $\delta^{13}\text{C}$  and  $\delta\text{D}$  in the last month of the campaign. One example is the improved temperature control of the trap during adsorption, which in turn stabilized the O<sub>2</sub> content in the measuring gas and thereby reduced variations in  $\delta^{13}\text{C}\text{-CH}_4$ .

9) L318: ERA interim

Done

10) L334: I presume this is following some spin up period? Are the delta-values at ~ steady state before the model run?

We did a long (20 years) spinup run for the year 2005. The atmospheric CH<sub>4</sub> growth rate had been stable for a few years then and thus it can be assumed that the atmosphere was relatively close to equilibrium with the emissions. We used this spinup as a starting point for our simulations, which cover the period 2005-2015. This way the imbalance of the atmospheric CH<sub>4</sub> and  $\delta^{13}\text{C}\text{-CH}_4$  in 2014 should be reasonably accounted for. The paragraph was modified accordingly as follows.

... source signatures (see Table 1). The emission inventory was built according to a double constraint: 1<sup>st</sup>, each source signature must be chosen within its own uncertainty interval, and 2<sup>nd</sup>, the resulting global average source signature must be compatible with the global source signature that is inferred from the observations (and that is known with a much better precision than the individual source signatures). In a second set of simulations, anthropogenic emissions in a regional domain centered on Cabauw were replaced by emissions from the European TNO-MACC\_2 inventory, which was used as the standard inventory in the FLEXPART-COSMO simulations (see below). Outside the regional domain covered by TNO-MACC\_2, the EDGAR emissions were used.

Atmospheric removal of CH<sub>4</sub> was modeled as described in Monteil et al. (2013), using kinetic fractionation factors  $\alpha = k(^{12}\text{C})/k(^{13}\text{C})$  of  $\alpha_{\text{OH}} = 1.0055$ ,  $\alpha_{\text{Cl}} = 1.0066$  and  $\alpha_{\text{O}(^1\text{D})} = 1.013$  for the reactions between CH<sub>4</sub> and OH (Sander et al., 2006), Cl (Saueressig et al., 1995) and O(<sup>1</sup>D) (Saueressig et al., 2000), respectively. The simulations were initialized at steady state (obtained via a spin-up run) in 2005, and simulations of the period 2005-2015 were used to calculate a realistic state of the atmosphere at the start of the measurement campaigns, including the imbalance between emissions and atmospheric CH<sub>4</sub> mixing ratio/isotopic composition in 2014. Time series were extracted from model-simulated mole fraction fields after interpolation to the horizontal coordinate and height of the Cabauw tower air inlet.

11) L369: This sentence is a little confusing and doesn't quite follow from the previous one. What was "done separately" for the SNAP categories?

To clarify this, the sentence on page 13 Line 369 was replaced by:

Methane mole fractions were computed separately for a number of SNAP (Standardized Nomenclature for Air Pollutants) source categories with specific isotopic signatures as summarized in Table 2.

12) L385: "This method allows ... to be determined"

Done



13) L429: I don't think "Inter-calibration" is the correct term here. I think you mean "Inter-comparison"? This section doesn't describe a calibration exercise.

Done

14) L466 and Figure 3: It looks to me like there is some non-linearity in the comparison between the two instruments for delta-D? The values at the lower end of the scale appear to be significantly lower for the TREX-QCLAS. Is this true? E.g. if a 2nd order polynomial were fit, it looks to me like it would come out with some curvature. I think this deserves a comment.

The response to this comment has been combined with the response to comment #19 of reviewer #1.

15) L498 - 499: TM5 does indeed seem to perform very well. However, I think this line is somewhat subjective (e.g. use of the term "remarkable") and should be removed.

Done

16) L508: I'm a little unclear what this line means. Do you mean simply that this offset is seen globally?

Yes, at least it is present in the whole Northern Hemisphere.

... offset by about 1 ‰, but this offset is also present at clean background sites in the Northern hemisphere.

17) L520: "showed, that" ... I don't think the comma is needed.

Done

18) L569 and Figure 7: I'm a little concerned about the points in Figure 7. My understanding of the MKP is that it is an hourly "running" 12-hour Keeling plot. Each point in Figure 7 is then the 6-hourly average of the "12-hour running intercepts". Therefore, it seems to me that what we're seeing at each point is a doubly smoothed estimate of the source signature during some ~ 18-hour period. Wouldn't this analysis be more transparent if a "normal" Keeling plot were calculated during a block 6 or 12-hour period? Otherwise it becomes more difficult to understand what these points really show and what time period they correspond to.

The reason for the additional 6-hour averaging is that in some cases the time periods of the MKP for  $\delta^{13}\text{C}$  and  $\delta\text{D}$  are not identical, e.g. because of instrument failure or because of the data filtering procedures. To increase the number of pairs of MKP intercepts the additional 6-hour averaging was added.

19) L644 - 645: delete "even"

Done

20) L654: This is a good example of where the term "source signatures" is confusing. I'm not sure whether you're referring to the particular isotopic ratio of the methane emitted from a source, or of something about the bulk source mix that you've inferred from the air mass.

This has been updated accordingly, see response to comment #2.

21) Figure 7: At the point where this Figure appears and is referenced, it's not clear what the "a" and "b" refer to in the event labels. I think the Figure caption should be expanded to explain when these events were.

The color coding, numbering and characters (a, b) of event labels of Figure 7 refer to Figure 9 as mentioned in the legend. In Figure 9 more details on the events are given. Nonetheless the additional information has also been added to Figure 7:

... Large colored symbols indicate data from the three events (event 1: 10<sup>th</sup> – 12<sup>th</sup> March, event 2: 16<sup>th</sup> – 18<sup>th</sup> March, event 3: 22<sup>nd</sup> to 24<sup>th</sup> March) that are highlighted in detail in Fig. 9. The labels a and b refer to day 1 and day 2 of the two-day events, respectively.

22) Figure 7: I think these points should have error bars.

Error bars have been added.

23) Figure 7: The reference to Rigby et al. (2012). The original “mean” values are from Snover et al (2000), which I think should be cited. The ranges are those assumed (somewhat arbitrarily) for the inversion in Rigby et al (2012).

The reference of Snover et al. (2000) was added to the legend of Figure 7:

... from recent literature (Snover et al., 2000; Rigby et al., 2012)



1 **In-situ observations of the isotopic composition of methane at the**  
2 **Cabauw tall tower site**

3

4 Thomas Röckmann<sup>1,\*</sup>, Simon Eyer<sup>2,\*</sup>, Carina van der Veen<sup>1</sup>, Maria E. Popa<sup>1</sup>, Béla  
5 Tuzson<sup>2</sup>, Guillaume Monteil<sup>1,3</sup>, Sander Houweling<sup>1</sup>, Eliza Harris<sup>2</sup>, Dominik  
6 Brunner<sup>2</sup>, Hubertus Fischer<sup>7</sup>, Giulia Zazzeri<sup>4</sup>, David Lowry<sup>4</sup>, Euan G. Nisbet<sup>4</sup>, Willi  
7 A. Brand<sup>5</sup>, Jaroslav M. Necki<sup>6</sup>, Lukas Emmenegger<sup>2</sup> and Joachim Mohn<sup>2</sup>

8

9 <sup>1</sup> Utrecht University (UU), Institute for Marine and Atmospheric Research  
10 Utrecht (IMAU), The Netherlands

11 <sup>2</sup> Empa, Laboratory for Air Pollution / Environmental Technology, Dübendorf,  
12 Switzerland

13 <sup>3</sup> now at Department of Physical Geography and Ecosystem Science, Lund  
14 University, Lund, Sweden

15 <sup>4</sup> Royal Holloway University of London (RHUL), Department of Earth Sciences,  
16 Egham, UK

17 <sup>5</sup> Max-Planck-Institute (MPI) for Biogeochemistry, Jena, Germany

18 <sup>6</sup> Environmental Physics Group, Faculty of Physics and Applied Computer  
19 Science, AGH University of Science and Technology, Krakow, Poland

20 <sup>7</sup> University of Bern, Climate and Environmental Physics, Bern, Switzerland

21

22 \*These authors contributed equally to this work

23

24

## Abstract

High precision analyses of the isotopic composition of methane in ambient air can potentially be used to discriminate between different source categories. Due to the complexity of isotope ratio measurements, such analyses have generally been performed in the laboratory on air samples collected in the field. This poses a limitation on the temporal resolution at which the isotopic composition can be monitored with reasonable logistical effort. Here we present the performance of a dual isotope ratio mass spectrometric system (IRMS) and a quantum cascade laser absorption spectroscopy (QCLAS) based technique for in-situ analysis of the isotopic composition of methane under field conditions. Both systems were deployed at the Cabauw experimental site for atmospheric research (CESAR) in the Netherlands and performed in-situ, high-frequency (approx. hourly) measurements for a period of more than 5 months. The IRMS and QCLAS instruments were in excellent agreement with a slight systematic offset of  $(+0.25 \pm 0.04) \text{ ‰}$  for  $\delta^{13}\text{C}$  and  $(-4.3 \pm 0.4) \text{ ‰}$  for  $\delta\text{D}$ . This was corrected for, yielding a combined dataset with more than 2500 measurements of both  $\delta^{13}\text{C}$  and  $\delta\text{D}$ . The high precision and temporal resolution dataset does not only reveal the overwhelming contribution of isotopically depleted agricultural  $\text{CH}_4$  emissions from ruminants at the Cabauw site, but also allows the identification of specific events with elevated contributions from more enriched sources such as natural gas and landfills. The final dataset was compared to model calculations using the global model TM5 and the mesoscale model FLEXPART-COSMO. The results of both models agree better with the measurements when the TNO-MACC emission inventory is used in the models than when the EDGAR inventory is used. This suggests that high-resolution isotope measurements have the potential to further constrain the methane budget, when they are performed at multiple sites that are representative for the entire European domain.

## 1. Introduction

The global increase of the important greenhouse gas methane in the atmosphere since the beginning of the industrial period is very well established (Dlugokencky et al., 2009; Dlugokencky et al., 1996; Dlugokencky et al., 1998; Etheridge et al., 1998; Khalil et al., 2007; Loulergue et al., 2008; MacFarling Meure et al., 2006; Rasmussen and Khalil, 1981; Spahni et al., 2005). The existing CH<sub>4</sub> mole fraction measurement data enable accurate assessment of the source-sink imbalance through time, and together with the estimated total sink strength, they allow for a top-down constraint on the global source of methane to the atmosphere (Bergamaschi et al., 2013; Houweling et al., 2014). Bottom-up estimates of the global methane budget carry much larger uncertainties, which are inherent to the assumptions made in the extrapolation of local scale measurements to larger scales (Bruhwiler et al., 2014; Kirschke et al., 2013; Nisbet et al., 2014). The advantage of bottom-up estimates is, however, the possibility to distinguish different sources and to link observations to process-level understanding of the emissions.

An independent approach for distinguishing between source categories of CH<sub>4</sub> is the analysis of its isotopic composition, which is strongly linked to the source/sink processes. This is particularly true for methane from biogenic, thermogenic and pyrogenic sources (Gros et al., 2004; Houweling et al., 2008; Quay et al., 1999; Sapart et al., 2012). A more detailed differentiation within one source category, e.g. biogenic CH<sub>4</sub>, for emissions from wetlands, ruminants, rice paddies or termites, however, is complicated because of the overlap of the respective isotopic source signatures. Further complications arise because individual source signatures can show pronounced dependence on environmental parameters and metabolized substrates (Kawagucci et al., 2014; Klevenhusen et al., 2010). In addition to the source contributions, the sink processes (mainly chemical removal by the hydroxyl radical (OH), but also soil deposition and stratospheric loss) also affect the isotopic composition of atmospheric methane (Brenninkmeijer et al., 1995; Röckmann et al., 2011; Saueressig et al., 1996; Saueressig et al., 2001; Snover and Quay, 2000). Nevertheless, over the past decades, numerous studies have shown the potential of isotope measurements to identify individual source categories from isotope

observations (Beck et al., 2012; Lassey et al., 1993; Tarasova et al., 2006; Umezawa et al., 2012b; Zazzeri et al., 2015) and to constrain budgets (Ferretti et al., 2005; Fischer et al., 2008; Houweling et al., 2008; Lassey et al., 2000; Lowe et al., 1994; Sapart et al., 2012; Umezawa et al., 2012a).

The isotopic composition is commonly reported in  $\delta$  notation, where  $\delta$  quantifies the relative deviation of an isotope ratio ( $^{13}R = ^{13}\text{C}/^{12}\text{C}$  for carbon isotopes and  $^2R = ^2\text{H}/^1\text{H}$ , abbreviated as D/H, for hydrogen isotopes) in a sample from a standard ratio. The international standard for reporting  $\delta(^{13}\text{C}, \text{CH}_4)$  values is Vienna Pee Dee Belemnite (VPDB,  $^{13}R_{\text{VPDB}} = 0.0112372$  (Craig, 1957)) and for  $\delta(\text{D}, \text{CH}_4)$  it is Vienna Standard Mean Ocean Water (VSMOW,  $^2R_{\text{VSMOW}} = 0.0020052$  (Baertschi, 1976)).  $\delta(^{13}\text{C}, \text{CH}_4)$  and  $\delta(\text{D}, \text{CH}_4)$  are abbreviated as  $\delta^{13}\text{C}$  and  $\delta\text{D}$  in the following, and given in per mill (‰).  $\text{CH}_4$  mole fractions  $\chi(\text{CH}_4)$  are reported in  $\text{nmol/mol} = 10^{-9}$  and  $\mu\text{mol/mol} = 10^{-6}$ . For interpretation of global or continental scale atmospheric data the expert group of the WMO/IAEA has set a scientifically desirable level of compatibility of 2 nmol/mol, 0.02 ‰ and 1 ‰ for  $\text{CH}_4$  fraction,  $\delta^{13}\text{C}$  and  $\delta\text{D}$ , respectively (WMO, 2014). For regionally focused studies with large local fluxes, extended compatibility goals of 5 nmol/mol, 0.2 ‰ and 5 ‰ for  $\chi(\text{CH}_4)$ ,  $\delta^{13}\text{C}$  and  $\delta\text{D}$  were defined.

Due to the complexity of the involved measurement techniques,  $\text{CH}_4$  isotope measurements have been limited mostly to relatively low frequency sampling in the field followed by isotope analysis in the laboratory (Bock et al., 2010; Brass and Röckmann, 2010; Sapart et al., 2011; Sperlich et al., 2013; Umezawa et al., 2009; Yamada et al., 2003). For many decades, the dominant method for high precision isotope analysis of atmospheric methane was isotope ratio mass spectrometry. In particular, the development of continuous-flow IRMS in the past two decades (Merritt et al., 1994; Merritt et al., 1995) has greatly increased the throughput of IRMS methods, making this the technique of choice in most laboratories, also because of the small sample amounts required.

Recently, mid-infrared laser absorption spectroscopy has proven its potential for high precision isotope ratio analysis. First attempts of measuring the isotopic composition of methane (Bergamaschi et al., 1998a; 1998b; 1994) were restricted to enhanced  $\text{CH}_4$  fractions ( $>50 \mu\text{mol/mol}$  for  $\delta^{13}\text{C}$  and  $>2000$

$\mu\text{mol/mol}$  for  $\delta\text{D}$ ) and required cryogenic cooling for both the laser source and the detector, which impeded in-situ and long-term applications. The invention of room temperature, quantum cascade laser (QCL) sources has triggered the development of a novel generation of spectrometers suitable for in-situ analysis of the isotopic composition of greenhouse gases (Eyer and al, 2015; Tuzson et al., 2008; Wächter et al., 2008). Their capability of high-temporal resolution led to new applications aiming for source attribution (Mohn et al., 2012; Tuzson et al., 2011; Wolf et al., 2015). The advantages of in-situ measurements are particularly apparent in combination with atmospheric modeling techniques, which enables the identification of specific source regions (Rigby et al., 2012; Sturm et al., 2013). Similarly, high-frequency, high-precision  $\text{CH}_4$  isotope data are expected to greatly reduce uncertainties of national and global source estimations, as demonstrated in an observing system simulation experiment (Rigby et al., 2012). In this paper we present the analytical setup and results of a 5-month campaign at the Cabauw tall tower site in the Netherlands, where the isotopic composition ( $\delta^{13}\text{C}$  and  $\delta\text{D}$ ) of  $\text{CH}_4$  was measured with two instruments, one IRMS system developed at Utrecht University and one QCLAS-instrument developed at Empa. The compatibility of the two analytical techniques for  $\text{CH}_4$  mole fractions,  $\delta^{13}\text{C}-\text{CH}_4$  and  $\delta\text{D}-\text{CH}_4$  is assessed and the obtained high-resolution isotope dataset is exploited using a novel moving Keeling plot method. A comparison of measurement results with calculations from two different models (TM5 and FLEXPART-COSMO) and two emission inventories (EDGAR, TNO-MACC) indicates the potential of this approach to better constrain on isotope source signatures and emissions in atmospheric models.

## 2. Methods

### 2.1. Site description

The 213 m tall tower is the central construction of the Cabauw Experimental Site for Atmospheric Research (CESAR, <http://www.cesar-observatory.nl/>,  $51^\circ 58' \text{ N}$ ,  $4^\circ 55' \text{ E}$ , 2 m a.s.l.). The CESAR site is dedicated to atmospheric research and hosts a wide variety of instruments for in situ and remote sensing measurements of meteorological parameters, trace gases, pollutants, aerosols, and clouds. The

site is located in an agricultural landscape, with CH<sub>4</sub> emissions originating from ruminants and other agricultural activities, but also from the peaty soil and the drainage ditches between the surrounding fields (Peltola et al., 2014). The small town Lopik (~7500 inhabitants) is located 1 km east of the tower. Population and road density increase steeply further away from the tower towards the country's major cities: Utrecht (at about 20 km distance), Rotterdam (30 km), the Hague (40 km) and Amsterdam (45 km). An estimated seven million people inhabit these cities and their many neighboring settlements. The location and surroundings are described in more detail in (Peltola et al., 2014; Peltola et al., 2015; Vermeulen et al., 2011). The instruments were operated in a room on the ground floor of the CESAR building. Since this room is not commonly used as laboratory, it has **air-conditioning with limited cooling capacity** and the temperature varied between 25 °C and 30 °C.

## **2.2. Air sampling at the Cabauw tall tower**

Air was continuously drawn through ½" o.d. **(outer diameter)** Dekabon tubing from 20 m height at a total flow of 16 l min<sup>-1</sup> provided by a **Varian scroll pump (Agilent Technologies Inc., USA)**. The sample gas flow was adjusted by means of a flow restriction at the inlet of the pump in order to maintain the pressure in the sampling line above 950 hPa. The sample gas flows for the methane isotope analyzers were branched off upstream of the scroll pump and the restriction, using ¼" o.d. Dekabon lines.

## **2.3. IRMS system**

The new IRMS method for δ<sup>13</sup>C and δD analysis of atmospheric CH<sub>4</sub> is based on the ISAAC system as developed at the MPI for Biogeochemistry in Jena (W. Brand et al., manuscript in preparation). Importantly, the system does not require liquid nitrogen coolant for the preconcentration and focusing steps, but uses a massive copper block cooled down to about -145 °C, to which the cold traps for preconcentration and cryo-focussing are connected via standoffs (see 2.3.1). This cold assembly is contained in an evacuated steel Dewar to prevent condensation of moisture. During the campaign, the extraction unit and two IRMS instruments (Thermo Delta Plus XL for hydrogen isotopes and Thermo Delta Plus XP for

carbon isotopes, both Thermo Fisher Scientific Inc., Germany) were operated at the CESAR site. The system is schematically shown in Fig. 1.

### 2.3.1. Cryogenic trapping

A Polycold compact cooler compressor (Brooks Automation Inc., USA), filled with coolant PT-30, cooled a cold end on which a copper cylinder (70 mm diameter, 85 mm height, 3 kg) was mounted. In this configuration, the copper block reached a temperature of -145 °C. The pre-concentration trap (PreCon) was a 10 cm 1/8" SS tube filled with 4 cm 60/80 mesh HayeSep D in the center and 3 cm 60/80 glass beads on each end. It was connected with Valco fittings and the packing material was retained in the trap using removable frits (CEF1F, Valco Instruments Company Inc., USA). The focus trap (Focus) was a 10 cm 1/16" SS tube filled with 2 cm HayeSep D and 4 cm glass beads at both ends, connected with Valco fittings (ECEF211.0F, Valco Instruments Company Inc., USA). The traps could be heated with 0.5 m Thermsys heating wire wrapped around the tubes. The PreCon and Focus trapping units were glued together with a PT-100 temperature sensor in heat - conducting two component epoxy on a brass standoff. These brass standoffs were mounted to the copper cylinder. In the "trapping" configuration the temperatures of the traps were usually kept at -135 °C.

### 2.3.2. Measurement procedure

A 3-port 2-position Valco valve (3PV, Fig. 1) selected either ambient air drawn from the tower through a  $\text{Mg}(\text{ClO}_4)_2$  dryer, or cylinder air that was injected via one port of an 8-port multiposition Valco valve (MPV). To check the system performance, a reference air cylinder (Ref) was measured alternately with ambient air, and three other target gas cylinders were measured occasionally. The inlet line was connected to a 4-port 2-position Valco valve (4PV1), which directed either Helium (He, BIP quality, Air Products and Chemicals Inc., USA) or the selected airflow to the PreCon unit, which was connected in the loop position of a 6-port 2-position Valco valve (6PV). All He and air flows were controlled by MKS mass flow controllers (MFC, MKS Instruments Inc., USA).

The preconcentration and cryofocussing was done similarly to Brass and



210 Röckmann (2010). After flushing the inlet line with >20 ml air, the 6PV was  
211 switched to the load position and air was admitted to the PreCon unit. The  
212 duration of the air sampling for the IRMS system was 10 minutes at a flow rate of  
213 5 ml min<sup>-1</sup> for  $\delta^{13}\text{C}$  and 7 ml min<sup>-1</sup> for  $\delta\text{D}$ . The flow was provided by a Xavitech  
214 mini pump (P200-GAS-12V, Xavitech AB, Sweden). During this step, the  
215 temperature measured at the PreCon stayed below -132 °C. At this temperature  
216 CH<sub>4</sub> and several other trace species were retained on the HayeSep D, while the  
217 air matrix was efficiently flushed out.

218 After preconcentration, the PreCon unit was heated to -30 °C and a He flow of  
219 3 ml min<sup>-1</sup> transported the CH<sub>4</sub> in 90 seconds to the Focus unit, which was held at  
220 a temperature <-137 °C. After transfer of the sample to the Focus, the 6PV was  
221 switched to the load position and the PreCon was heated to -10 °C to release any  
222 remaining trapped gases such as CO<sub>2</sub>.

223 The Focus was then heated to release the CH<sub>4</sub>, which was directed via 4PV2 and  
224 4VP3 either to the combustion oven and the Delta plus XP IRMS for <sup>13</sup>C analysis  
225 or to the pyrolysis oven and the Delta plus XL IRMS for D analysis.

226 For  $\delta\text{D}$  analysis, the CH<sub>4</sub> was injected into a pyrolysis tube furnace (1400 °C),  
227 where CH<sub>4</sub> was converted to H<sub>2</sub> and carbon. The H<sub>2</sub> entered the IRMS, after  
228 passing a 2 m CarboPLOT column at room temperature (RT) and a nafion dryer,  
229 via the GasBench interface. No krypton interference (Schmitt et al., 2013) could  
230 be determined in this setup. The repeatability for  $\delta\text{D}$  was generally better than  
231  $\pm 2$  ‰ (reported as SD), based on consecutive analyses of reference air.

232 For  $\delta^{13}\text{C}$ , the CH<sub>4</sub> was injected from the cryofocus unit into a combustion oven  
233 containing a nickel / nickel oxide wire catalyst at 1100 °C, where the CH<sub>4</sub> was  
234 converted to CO<sub>2</sub> and H<sub>2</sub>O. The resulting gas mixture passed a nafion dryer and a  
235 10 m PoraPLOT Q column (5 °C) to eliminate interference from co-trapped  
236 krypton (Schmitt et al., 2013) before entering the IRMS via the GasBench  
237 interface. The repeatability of  $\delta^{13}\text{C}$  was better than  $\pm 0.07$  ‰ (reported as SD),  
238 based on consecutive analyses of reference air.

239 The typical measurement order during the Cabauw campaign was Ref  $\delta^{13}\text{C}$  – Air  
240  $\delta^{13}\text{C}$  – Ref  $\delta\text{D}$  – Air  $\delta\text{D}$ . A full measurement cycle took 84 min. On a regular basis,  
241 pressurized air from a cylinder, applied as a target gas, was analyzed as a quality

control tool in order to monitor the long term stability of the analytical technique. The CH<sub>4</sub> mole fraction and isotopic composition in ambient air and target gas were calculated using an interpolation of the reference air analyzed before and afterwards. A custom made LabView software program (National Instruments Corp., USA) was used to control and log the temperature of the traps, the valve switching and the flow setpoints of the MFCs.

### 2.3.3. IRMS system isotope calibration

The isotope calibration of the IRMS system was based on a reference air cylinder that contains ambient air collected at the IMAU in 2014, with 1888 nmol/mol of CH<sub>4</sub> and isotope values of  $\delta^{13}\text{C} = -47.89 \text{ ‰}$  and  $\delta\text{D} = -88.08 \text{ ‰}$ . The isotope calibration scale is based on the reference scale that was described in detail in Brass and Röckmann (2010). We used the average of the reference air measurement before and after the sample air measurement to calculate the mole fraction and  $\delta$  values. The linear response of the analytical system (independence of the  $\delta$  value on the amount of CH<sub>4</sub> analyzed) was verified by injecting various volumes of reference air up to a volume equivalent to 2700 nmol/mol. Occasionally, the long-term stability of the system was checked by measuring 3 target cylinders with different CH<sub>4</sub> mole fractions and isotopic compositions. A robust link of the isotopic composition to the international reference materials VPDB and VSMOW has been established in the framework of the INGOS project (Sperlich et al., 2016).

### 2.4. QCLAS system

The analytical procedure of the laser based measurement system involves two steps: preconcentration of the CH<sub>4</sub> from 7.5 L of ambient air in a trace gas extractor (TREX) by adsorption on HayeSep D (Eyer et al., 2014; Mohn et al., 2010) and analysis of CH<sub>4</sub> isotopologues with a modified commercial QCLAS (QCL-76-D, Aerodyne Inc., USA). Details on the development, optimization and validation of the TREX-QCLAS system are given by Eyer et al. (2015).

The present manuscript comprises the first application of the TREX-QCLAS system for in-situ analysis of CH<sub>4</sub> isotopologues at a field site for an extended period of time. In comparison to the original setup, the heating power of the

polyimide foil on the cold trap was reduced to 60 W to increase its lifetime. Due to the lower heating power, the duration of the desorption step had to be extended, which led to an improved separation from residual bulk gases (e.g. N<sub>2</sub> and O<sub>2</sub>). Lowering the O<sub>2</sub> enhancement in the gas matrix is also the main reason for a lower offset in  $\delta^{13}\text{C}$  of 1.58 ‰, with respect to the MPI - scale, as compared to 2.3 ‰ in previously published results (Eyer et al., 2015). The offset was related to a higher O<sub>2</sub> mole fraction in the gas matrix after CH<sub>4</sub> preconcentration. One measurement cycle consisted of four consecutive measurements of ambient air samples and one sample of pressurized air used as a target gas, followed by a calibration phase and took around 4:30 hours. This translates into an analysis time of 54 minutes per sample of ambient or pressurized air.

A calibration gas (CG1,  $(1200 \pm 50)$   $\mu\text{mol/mol}$  CH<sub>4</sub>,  $\delta^{13}\text{C} = -(44.24 \pm 0.10)$  ‰,  $\delta\text{D} = -(104.7 \pm 1.1)$  ‰) was diluted to 688  $\mu\text{mol/mol}$  and analyzed between every preconcentrated sample as an anchor to correct the measurements for instrumental drift. A second calibration gas (CG2,  $(1103.8 \pm 3.5)$   $\mu\text{mol/mol}$  CH<sub>4</sub>,  $\delta^{13}\text{C} = -(36.13 \pm 0.10)$  ‰,  $\delta\text{D} = -(180.6 \pm 1.1)$  ‰), diluted to a similar CH<sub>4</sub> mole fraction of 681  $\mu\text{mol/mol}$  was used to calculate calibration factors for  $\delta^{13}\text{C}$  and  $\delta\text{D}$  values. Furthermore, gas cylinders of pressurized ambient air, referred to as target gas (TG1, TG2), were frequently measured over the entire campaign to determine and verify the repeatability of the measurement system, which was found to be 0.28 ‰ and 1.7 ‰ for  $\delta^{13}\text{C}$  and  $\delta\text{D}$  (1 $\sigma$ ), respectively. Additional adjustments in the preconcentration procedure and in the analytical routine for isotope analysis improved the repeatability to 0.18 ‰ and 0.85 ‰ for  $\delta^{13}\text{C}$  and  $\delta\text{D}$  in the last month of the campaign. One example is the improved temperature control of the trap during adsorption, which in turn stabilized the O<sub>2</sub> content in the measuring gas and thereby reduced variations in  $\delta^{13}\text{C}$ -CH<sub>4</sub>.

The CH<sub>4</sub> isotopic composition of the calibration gases, as well as the target gases (TG1,  $(2639.5 \pm 0.6)$  nmol/mol CH<sub>4</sub>,  $\delta^{13}\text{C} = -(46.48 \pm 0.10)$  ‰,  $\delta\text{D} = -(119.0 \pm 1.1)$  ‰, TG2,  $(2659.8 \pm 0.6)$  nmol/mol CH<sub>4</sub>,  $\delta^{13}\text{C} = -(45.87 \pm 0.10)$  ‰,  $\delta\text{D} = -(114.1 \pm 1.1)$  ‰) were determined by the Stable Isotope Laboratory at the Max-Planck-Institute for Biogeochemistry. CH<sub>4</sub> mole fraction measurements were linked to

the WMO-X2004 calibration scale (Dlugokencky et al., 2005) through calibration of the target gases against NOAA reference standards at Empa.

## **2.5. Modeling**

Two complementary atmospheric transport models (TM5, FLEXPART-COSMO), both in combination with two different emissions inventories (TNO-MACC\_2, EDGAR/LPJ-WhyMe), were applied to support interpretation of the measurements. The Eulerian tracer model TM5 simulated the distribution of CH<sub>4</sub> and <sup>13</sup>CH<sub>4</sub> at global scale with a zoom on Europe at 1° x 1° resolution and considered both the isotopic signatures of different sources and the fractionation by different removal pathways of CH<sub>4</sub> in the atmosphere. The Lagrangian particle dispersion model FLEXPART-COSMO, conversely, was run in backward mode at a higher resolution of 0.06° x 0.06° but only over Europe. This model is better able to represent the spatial variability of CH<sub>4</sub> sources in the near field of Cabauw but it only simulated the contributions from the last 4 days of emissions within Europe and not the large-scale background. Chemical loss of CH<sub>4</sub> was not considered due to the short transport times between the sources and the receptor point at Cabauw. δD was only simulated with FLEXPART-COSMO.

### **2.5.1. TM5 modeling**

Simulations of atmospheric CH<sub>4</sub> and δ<sup>13</sup>C were performed using the global tracer model TM5 (Krol et al., 2005). The Eulerian off-line model was driven by meteorological fields from the European Centre for Medium Range Weather Forecast (ECMWF) reanalysis project ERA-Interim (Dee et al., 2011), pre-processed for use in TM5. For vertical transport due to moist convection we made use of Era Interim archived convective mass fluxes, replacing the use of the Tiedke scheme in Krol et al. (2005). The model was run at a horizontal resolution of 6°x4° globally and 1°x1° inside a zoom domain covering Western Europe. The model uses 25 hybrid sigma-pressure levels from the surface to top of atmosphere.

Two parallel (forward) TM5 simulations were performed with CH<sub>4</sub> and <sup>13</sup>CH<sub>4</sub> as transported tracers. In the standard configuration, anthropogenic CH<sub>4</sub> emissions were taken from EDGAR4.2 FT2010 (EDGAR, 2009), extrapolated to 2014 and

2015 using annual statistics from the Food and Agriculture Organization of the United Nations (FAO) and the British Petroleum Company (BP), as described in Houweling et al. (2014). For natural wetland emissions, an average of the emission estimates derived by Spahni et al. (2011) for the period 2003-2008 was taken, using the LPJ-WhyMe model. For a complete description of the CH<sub>4</sub> emissions (Table 1), see Monteil et al. (2013) and references therein. <sup>13</sup>CH<sub>4</sub> emissions were derived from the CH<sub>4</sub> emissions using prescribed  $\delta^{13}\text{C}$  source signatures (Table 1). The emission inventory was built according to a double constraint: 1<sup>st</sup>, each source signature must be chosen within its own uncertainty interval, and 2<sup>nd</sup>, the resulting global average source signature must be compatible with the global source signature that is inferred from the observations (and that is known with a much better precision than the individual source signatures) (Monteil et al., 2011). In a second set of simulations, anthropogenic emissions in a regional domain centered on Cabauw were replaced by emissions from the European TNO-MACC\_2 inventory, which was used as the standard inventory in the FLEXPART-COSMO simulations (see below). Outside the regional domain covered by TNO-MACC\_2, the EDGAR emissions were used.

Atmospheric removal of CH<sub>4</sub> was modeled as described in Monteil et al. (2013), using kinetic fractionation factors  $\alpha = k(^{12}\text{C}) / k(^{13}\text{C})$  of  $\alpha_{\text{OH}} = 1.0055$ ,  $\alpha_{\text{Cl}} = 1.066$  and  $\alpha_{\text{O}(1\text{D})} = 1.013$  for the reactions between CH<sub>4</sub> and OH (Sander et al., 2006), Cl (Saueressig et al., 1995) and O(<sup>1</sup>D) (Saueressig et al., 2000), respectively. The simulations were initialized at steady state (obtained via a spin-up run) in 2005, and simulations of the period 2005-2015 were used to calculate a realistic state of the atmosphere at the start of the measurement campaigns, including the imbalance between emissions and atmospheric CH<sub>4</sub> mixing ratio/isotopic composition in 2014. Time series were extracted from model-simulated mole fraction fields after interpolation to the horizontal coordinate and height of the Cabauw tower air inlet.

### 2.5.2. FLEXPART-COSMO modeling

The Lagrangian Particle Dispersion Model (LPDM) FLEXPART (Stohl et al., 2005) was used in a modified version coupled to the mesoscale numerical weather

forecast model COSMO (Baldauf et al., 2011) to simulate the regional contribution of different source categories to the concentrations and isotopic signatures of CH<sub>4</sub> at Cabauw. FLEXPART-COSMO was driven by hourly operational analysis fields generated by the Swiss national weather service MeteoSwiss for a domain covering entire western and central Europe from Ireland, Denmark, and Poland in the north to Portugal and southern Italy in the south with a horizontal resolution of approximately 7 km x 7 km and 60 vertical levels. Every 3 hours, 50'000 particles (air parcels) were released from the position of the inlet 20 m above surface and traced backward in time for 4 days to compute the sensitivity of each 3-hourly measurement to upwind sources. The corresponding source sensitivity maps or footprints (Seibert and Frank, 2004) were multiplied with gridded CH<sub>4</sub> emissions to compute the mole fraction enhancement above background expected from different sources. Emissions were taken from the TNO-MACC\_2 inventory for Europe representative of the year 2009 and available at 0.125° x 0.0625° resolution (Kuenen et al., 2014) or, alternatively, from the same version of EDGAR/LPJ-WhyMe inventory driving TM5 at a resolution of 1° x 1°. Methane mole fractions were computed separately for a number of SNAP (Standardized Nomenclature for Air Pollutants) source categories with specific isotopic signatures as summarized in Table 2.

For the domain covered by the FLEXPART-COSMO simulations, which includes most of western and central Europe, total anthropogenic emissions are 20.6 Tg CH<sub>4</sub>/yr in EDGAR and 18.3 Tg CH<sub>4</sub>/yr in TNO-MACC, which corresponds to a difference of 12.5%. CH<sub>4</sub> emissions from gas/oil production and distribution are 89% higher, CH<sub>4</sub> emissions from agriculture 19% lower and CH<sub>4</sub> emissions from waste 12% higher in EDGAR than in TNO-MACC.

Source specific emissions were combined with isotopic signatures of the various categories from Table 2 to derive mean  $\delta^{13}\text{C}$  and  $\delta\text{D}$  isotopic signatures for the CH<sub>4</sub> that was picked up by the air parcel along the trajectory.

## 2.6. Interpretation of CH<sub>4</sub> isotope data

### 2.6.1. Data analysis by a Keeling plot technique

The isotopic composition of CH<sub>4</sub> emissions were estimated using the Keeling plot technique (Keeling, 1961; Pataki et al., 2003). This method allows the isotopic signature of a single source process or the mean isotopic signature of combined source processes that mix into a background reservoir to be determined from the observed ambient isotopic composition and mole fraction. An implicit assumption of the Keeling plot approach is that the isotopic composition and mole fraction of the background reservoir and the isotopic composition of the source or the combined source stay constant over the time range of the analysis. This may not always apply as the relative contribution of individual CH<sub>4</sub> sources or their isotopic signature may change over time

To exploit the high temporal resolution of our data, we applied a novel approach of a moving Keeling plot (MKP) method. Data within a moving window of 12 hours were used to calculate the source isotopic composition. This window was moved in 1-hour time steps over the data series. In addition, values for background conditions within a 48-hour period, centered on the respective 12-hour window, were included in the analysis. These background values were chosen between 10:00 and 18:00 local time, because during this period a convective boundary layer usually develops and hence local influence is weak; pollution events with CH<sub>4</sub> mole fractions above 2100 nmol/mol were filtered out additionally. For each time window, an orthogonal least squares fit was applied to the  $\delta$  values vs. the inverse CH<sub>4</sub> mole fractions and R<sup>2</sup> values were calculated. A Keeling plot analysis only returns meaningful values for the source isotopic composition if the variations in CH<sub>4</sub> mole fraction are significant and if the emissions are from a source with a well-defined isotopic composition. Therefore, two additional filters were applied: i) the mole fraction had to vary by more than 200 nmol/mol within each time window and ii) the R<sup>2</sup> of the fit had to be larger than 0.8. If R<sup>2</sup> < 0.8, the 12 h interval was reduced consecutively by one hour to a minimum of six hours until either the R<sup>2</sup> of the fit was > 0.8 or the number of data points was lower than five. On average this technique accumulated 22 data points per 12-h time window.

### 3. Results

#### 3.1. Overview of the field measurements at the Cabauw site



The full record of the methane mole fraction and isotopic composition obtained with the two measurement techniques at the CESAR site is shown in Fig. 2. The IRMS system started with  $\delta\text{D}$  measurements first, and after 3 weeks delivered both  $\delta^{13}\text{C}$  and  $\delta\text{D}$  data. The TREX-QCLAS system started later and ran continuously from mid-December to mid-January, and from mid-February to the end of the campaign. Despite a number of interruptions mainly due to various kinds of instrument malfunction, the combined time series of both techniques shows a high temporal coverage with more than 2500 measurements performed for both  $\delta^{13}\text{C}$  and  $\delta\text{D}$ .

A qualitative inspection of the time series already conveys the obvious features that will be discussed below in more detail: the methane mole fraction  $\chi(\text{CH}_4)$  shows a large number of substantial increases above background level, and these positive methane excursions are accompanied by negative excursions in the  $\delta$  values from the background level. Thus the additional methane is generally depleted in both  $^{13}\text{C}$  and D.

### 3.2. **Inter-comparison** of the two analytical techniques

Before presenting a detailed analysis of the  $\text{CH}_4$  isotopic composition in ambient air, we compare the results obtained with the IRMS and QCLAS techniques in order to evaluate their performance and to combine the results into one final dataset. Although both systems measured air from the same intake line, the sampling intervals could not be synchronized since both instruments operated in different measurement cycles. A full measurement cycle (including measurement of the reference gas) took 84 minutes for the IRMS system and 54 minutes for the TREX-QCLAS system. The actual duration of the air sampling was 10 minutes for the IRMS system and 15 minutes for the QCLAS system. So even if the systems coincidentally started sampling at the same time, they never actually analyzed exactly the same air mass. Consequently, differences between the systems contain contributions from natural variability, random fluctuations due to limited measurement precision, and system offsets.

Fig. 3 shows a comparison of the  $\chi(\text{CH}_4)$ , as well as  $\delta^{13}\text{C}$  and  $\delta\text{D}$  values that were obtained with the TREX-QCLAS and the IRMS technique. To visualize the possible effect of time shifts, the size of the points corresponds to the proximity of the

sampling intervals. A total of 727, 333 and 277 measurement pairs for  $\chi(\text{CH}_4)$ ,  $\delta^{13}\text{C}$  and  $\delta\text{D}$ , respectively, analyzed by both techniques were combined in this way.

The mole fraction comparison shows good agreement along the 1:1 line but with a large scatter, which has two contributions: i) instrumental noise, as the isotope systems have a relatively large uncertainty for measurement of the mole fraction compared to existing high-precision  $\text{CH}_4$  analyzers, and ii) natural variability associated with the sampling of different air masses as described above. The second point is supported by the fact that the average difference in  $\text{CH}_4$  mole fractions between the two analytical techniques was larger for larger temporal differences in the sampling intervals.

For the isotope intercalibration plots, the grey-black shading of the circles indicates the difference in  $\chi(\text{CH}_4)$  of the respective measurement pair analyzed by both techniques. The overall difference between the measurements conducted with the two systems (QCLAS-IRMS) is  $(+0.25 \pm 0.04) \text{ ‰}$  for  $\delta^{13}\text{C}$  and  $(-4.3 \pm 0.4) \text{ ‰}$  for  $\delta\text{D}$  (the stated errors are standard errors of the mean). The mean offsets are slightly outside the WMO extended compatibility goals for  $\delta^{13}\text{C}$  ( $0.2 \text{ ‰}$ ) and within the WMO extended compatibility goals for  $\delta\text{D}$  ( $5 \text{ ‰}$ ), as indicated by the red dashed lines (WMO, 2014). Individual measurement pairs can show significantly larger deviations for aforementioned reasons. Differences between the two techniques are higher than expected as both laboratories refer their measurements to MPI-BGC, who recently established a link between the  $\text{CH}_4$  isotopic composition and the international reference materials VPDB and VSMOW, in the framework of the INGOS project (Sperlich et al., 2016). Therefore, remaining differences can only be rationalized by uncertainties in propagating the scale or by instrumental issues. The enhanced discrepancies for low  $\delta\text{D}$ - $\text{CH}_4$  values might originate from a non-linear response of one of the applied analytical techniques. The mean offset values determined above were applied to the QCLAS data to create one combined dataset with 2610 data points for  $\delta^{13}\text{C}$  and 2673 data points for  $\delta\text{D}$ .

### 3.3. FLEXPART-COSMO source attribution

In FLEXPART-COSMO, the contributions of the individual source types are simulated separately and added up to obtain the cumulative CH<sub>4</sub> mole fraction. Fig. 4 shows these contributions in absolute (top) and relative terms (bottom). According to the model, the relative contributions at the Cabauw site are quite uniform, with agricultural sources accounting for more than 60%, waste (mostly landfills) around 20–40%, and fossil sources between 0 and 40%. We note that significant contributions from fossil sources are only detected episodically, during several events that usually last a few days. Contributions from other source categories are generally negligible at the Cabauw site.

### 3.4. TM5 and FLEXPART-COSMO modeling including isotopes

The TM5 model calculates the combined influence of the global methane sources and sinks on CH<sub>4</sub> and  $\delta^{13}\text{C}$  at the Cabauw tower, and therefore the TM5 results can be compared directly to the measured time series. For FLEXPART-COSMO, a representative background mole fraction and isotopic signature needs to be added for comparison with the observations. For simplicity we assumed a constant background similar to the observed values for background conditions: 1930 nmol/mol for  $\chi(\text{CH}_4)$  with  $\delta^{13}\text{C} = -47.1 \text{ ‰}$  and  $\delta\text{D} = -86 \text{ ‰}$ .

Fig. 5 shows a comparison of these model-generated time series with the measured data for the entire campaign. Both models capture the amplitude and the temporal variability of  $\chi(\text{CH}_4)$  well. Most of the methane pollution events observed at the CESAR site are also present in the modeled time series and the increase in  $\chi(\text{CH}_4)$  is of a comparable size. In addition, the results of the TM5 and the FLEXPART-COSMO model for CH<sub>4</sub> mole fractions agree relatively well with each other ( $R^2=0.69$ ), in particular when both models are run with the same inventory at the same coarse spatial resolution, i.e. with EDGAR/LPJ-WhyMe.

A few pronounced CH<sub>4</sub> events in Fig. 5 show larger differences between the models. On 2 November, FLEXPART-COSMO simulates an emission signal that is not captured by TM5. Unfortunately no measurements are available for this event to decide on which model performs better. On 30 November TM5 simulates a CH<sub>4</sub> plume, which is absent in FLEXPART-COSMO, and this event is also not supported by the measurements. The global model has the advantage

that it includes the influence of long-range transport. As expected, however, the observed variability is predominantly influenced by local and regional emissions. Regarding the time series of the  $\delta$  values, both TM5 and FLEXPART-COSMO qualitatively display the expected anti-correlations between  $\text{CH}_4$  and  $\delta^{13}\text{C}$ . However, the amplitude of the  $\delta^{13}\text{C}$  variability is generally underestimated in the model runs, especially when using the EDGAR inventory. In addition, the modeled background level of  $\delta^{13}\text{C}$  in TM5 is offset by up to 1 ‰, but this offset is also present at clean background sites in the Northern hemisphere.

Using the TNO-MACC inventory in FLEXPART-COSMO results in better agreement with the observed variability of  $\delta^{13}\text{C}$ . In TM5, the TNO-MACC emissions reduce the amplitude of the  $\text{CH}_4$  variability, which is explained by the 13% lower emissions in TNO-MACC compared with EDGAR. Furthermore, the results of both models are consistent with the emissions being more depleted in  $\delta^{13}\text{C}$  in TNO-MACC than in EDGAR. The measurements indicate emissions that are even more depleted in  $\delta^{13}\text{C}$  than TNO-MACC values. These results suggest that the fractional contribution of isotopically heavy fossil emissions is overestimated in EDGAR, at least in the area sampled by Cabauw, although the uncertainty in the assumed  $\delta^{13}\text{C}$  source signatures could also contribute. For instance, recent literature showed that landfill emissions from the UK are more depleted in  $^{13}\text{CH}_4$  due to the implementation of gas extraction systems (Zazzeri et al., 2015).

The  $\delta\text{D}$  time series simulated with FLEXPART-COSMO using the TNO-MACC inventory is in good agreement with the measurements. This further indicates that TNO-MACC has a realistic source mixture, but the uncertainties in the mean  $\delta\text{D}$  signature are too large to draw firm conclusions at this stage. Despite these uncertainties, Fig. 5 clearly demonstrates how isotopic measurements highlight differences between emission inventories, which would go unnoticed looking only at  $\text{CH}_4$  mole fractions. Additional information may be available from the combination of both isotope signatures. For several of the  $\text{CH}_4$  elevation events shown in Fig. 5b, the relative changes in  $\delta^{13}\text{C}$  and  $\delta\text{D}$  modeled with FLEXPART-COSMO vary when using the two different inventories (TNO-MACC and EDGAR). Some of the anomalies show differences pointing in the same direction for  $\delta^{13}\text{C}$

and  $\delta D$ , and some others not. This suggests that  $\delta D$  provides additional independent information, which will be discussed in more detail in Section 4.3 using a double isotope plot of the source signatures (Fig. 7). The benefit of the high-resolution dual isotope measurements for validating emissions used in the models will be investigated in Section 4.4.

## 4. Discussion

### 4.1. Diurnal and synoptic variability

A prominent feature of the high-resolution dataset is the pronounced diurnal variability, with large increases in  $CH_4$  mole fraction that occur often during the night, due to the shallow planetary boundary layer. In addition, there are also several synoptic (but much smaller) pollution events, where  $CH_4$  mole fractions stay above the unpolluted background level for several days. These elevations are likely caused by synoptic scale advection of  $CH_4$  plumes from other source regions with a different source mix.

### 4.2. Isotope identification of the mean $CH_4$ source

In Fig. 6, the Keeling plot technique is applied to identify the mean isotopic signatures ( $\delta^{13}C$ ,  $\delta D$ ) of the combined  $CH_4$  emissions detected at the Cabauw site. An orthogonal regression method was applied to determine the fit parameters. This analysis yields well-defined mean isotopic signatures of the cumulative source (the y-intercept of the regression analysis) of  $\delta^{13}C = -(60.8 \pm 0.2) \text{‰}$  and  $\delta D = -(298 \pm 1) \text{‰}$ . The inferred mean isotopic signature agrees well with emission from ruminants, which are expected to be the main source of  $CH_4$  in this rural area. This is plausible, because the mean isotopic signature is largely determined by the pronounced nighttime  $CH_4$  elevations, which represent the local emissions close to the tower. Also the source contributions modeled by FLEXPART-COSMO suggest the dominant influence of agricultural emissions in this rural area (Fig. 4). Interestingly, the mean isotopic signature for the much smaller synoptic  $CH_4$  variations of the background (red points in Fig. 6) is not significantly different from the one for the complete dataset.

### 4.3. Short-term variability

Given the high temporal resolution of the dataset presented here, the isotope variations can be interpreted in much more detail than the overall analysis performed above. This allows identifying varying contributions of CH<sub>4</sub> sources during different periods of the campaign. To do so, we applied a 12-hour Moving Keeling Plot (MKP) method to the data, as described in Sect 2.6.1.

Fig. 7 summarizes the results of the MKP method in the form of a  $\delta D$  vs.  $\delta^{13}C$  plot. To combine  $\delta^{13}C$  and  $\delta D$  measurements performed at different times, MKP intercepts were averaged over 6 h intervals. Mean  $\delta^{13}C$  signatures range between -68 ‰ and -55 ‰ and mean  $\delta D$  signatures cover a relatively wide range between -350 ‰ and -260 ‰, indicating emissions mainly from microbial sources as derived from the cumulative Keeling plot analysis. During some periods, however, elevated mean  $\delta^{13}C$  and  $\delta D$  signatures reveal significant additional contributions from waste and/or fossil emissions.

The colored symbols in Fig. 7 highlight the mean isotopic signatures of three 48 h events (10-12, 16-18 and 22-24 March) that are discussed in more detail in the following. For the event of 16-18 March, selected results of the 12 h MKP method are displayed in Fig. 8, demonstrating the advantage of the high temporal resolution data. It is possible to clearly distinguish variations in the mean isotopic signatures during this event by variations in the y-axis intercepts. The increase by about 6 ‰ for  $\delta^{13}C$  and about 50 ‰ for  $\delta D$ , in the source isotopic signature for this event, clearly indicates the gradually increasing contribution of CH<sub>4</sub> from isotopically enriched sources, e.g. fossil fuel- or waste-related CH<sub>4</sub>.

The temporal evolution of the observed source mixture is investigated in further detail in Fig. 9, where the 16-18 March period (labeled as 2) is compared to two other 48 h – periods (10-12 March; label 1, and 22-24 March; label 3), each with significant diurnal CH<sub>4</sub> elevations. For event 1, the mean isotopic signatures stayed rather constant at values around  $\delta^{13}C = -63$  ‰ and  $\delta D = -320$  ‰. These values are typical for microbial emissions from an agricultural source and agree well with the source contributions predicted for this period by the FLEXPART-COSMO model.

Period 2 is characterized by much stronger isotopic change within the 48 h period. The  $\delta^{13}C$  signature increases to above -60 ‰ and the  $\delta D$  signature

increases to -240 ‰ by the end of the period (see Fig. 9). The double-isotope plot in Fig. 7 shows that the change in  $\delta D$  during event 2b clearly points towards fossil fuel sources, which provides independent support for the FLEXPART-COSMO simulations, where the contributions from fossil-fuel- derived emissions are higher for the second day.

For period 3, the mean  $\delta^{13}C$  isotopic signatures increased during the 48 h by about 2-3 ‰, whereas the  $\delta D$  signatures remained constant around -300 ‰. For this period, the double isotope plot of Fig. 7 indeed shows a shift towards the waste category. Also this observation is independently confirmed (at least qualitatively) by the FLEXPART-COSMO model derived source attribution, which indicates the largest fraction of waste-derived  $CH_4$  for the first day and a small addition of fossil  $CH_4$  for the second day of event 3. These examples show that even at a location like Cabauw, where one source category strongly dominates, contributions from isotopically different sources can be identified if sufficiently high-resolution dual isotope ratio data are available. We note that the “directional” information in the double isotope plot is only available by combining  $\delta^{13}C$  and  $\delta D$  measurements. It would be much harder, if not impossible, to detect an addition from fossil fuel- or landfill- derived  $CH_4$  based on  $\delta^{13}C$  or  $\delta D$  data alone.

#### **4.4. Evaluation of emission databases with high temporal resolution $CH_4$ isotope data**

As described in Section 3.4, both the TM5 and the FLEXPART-COSMO model-generated time series of  $CH_4$  mole fractions show an adequate agreement with the  $CH_4$  measurements at the Cabauw site. Therefore, the comparison between measurement data and the models can be used to evaluate the methane budget in more detail. In this context, the measured and modeled isotopic composition can be employed to assess the validity of emission inventories, EDGAR and TNO-MACC, with respect to the magnitude and spatial distribution of source categories. To compare the measured mean isotopic signatures to the model results, the simulated isotope time series were linearly interpolated and evaluated in the same way as the observations using the 12 h MKP method. This analysis was performed for both models (TM5 and FLEXPART-COSMO), each



using both the EDGAR/LPJ-Why-Me and the TNO\_MACC inventories. Additionally, time series for the mean isotopic signatures were calculated directly from FLEXPART-COSMO data, without using of the MKP method. This direct method allowed an independent estimation of the mean isotopic signatures and, thus, also provided an opportunity to evaluate the MKP method.

The statistics of the mean isotopic signatures from all four model-inventory combinations are shown as histograms in Fig. 10, together with the measurement-derived mean isotopic signatures and the directly derived signatures from FLEXPART-COSMO modeling. A clear difference can be observed between the mean isotopic signatures derived with the two different emission inventories. Model runs with the EDGAR/LPJ-WhyMe emission inventory (red in Fig. 10) tend to produce mean CH<sub>4</sub> isotopic signatures that are more enriched in <sup>13</sup>C and D than the model runs with TNO-MACC emissions. These differences are very similar for the simulations using TM5 and FLEXPART-COSMO, suggesting that differences originate from the emission inventories, rather than from differences between the models themselves. The δ<sup>13</sup>C source signatures derived from the measurements at the Cabauw tower are significantly more depleted than any of the model-generated datasets. For δD, the mean isotopic signatures using TNO-MACC emissions are relatively close to the measurements at Cabauw, whereas the values using EDGAR emissions are much more enriched in CH<sub>3</sub>D.

The high temporal resolution isotope data that are described in this paper thus provide relevant information to further constrain models and/or emission inventories, because the mean isotopic signatures can change rapidly. The comparison of our first high-resolution isotope measurements at Cabauw to model calculations clearly identify differences between the modeled inventories, where the EDGAR inventory produced too enriched mean isotopic signatures due to a higher contribution from fossil fuel sources. Similar differences in terms of source contributions between EDGAR and TNO-MACC\_2 were also reported by Hiller et al. (2014) for Switzerland, and Henne et al. (2015) concluded that natural gas emissions in Switzerland are likely overestimated in EDGAR.

## 5. Conclusions and outlook

The dual isotopic composition of CH<sub>4</sub> has been monitored for the first time with high temporal resolution in an extended (5 months) field deployment with two different instruments, an IRMS system and a QCLAS system, at the tall tower site Cabauw, the Netherlands. The measurements of both instruments compare well and can be combined to a time series of more than 2500 measurements for both  $\delta^{13}\text{C}$  and  $\delta\text{D}$ . Using a moving Keeling plot technique, the mean isotopic signatures of periods with significant CH<sub>4</sub> elevations can be derived with high temporal resolution. The combination of  $\delta^{13}\text{C}$  and  $\delta\text{D}$  data provides strong constraints to distinguish emissions from different source categories. Overall, CH<sub>4</sub> emissions at the Cabauw tall tower are dominated by agricultural sources, but variations in the mean isotopic signatures allow identification of events with increased contributions from fossil fuel and waste sources, which can be used to validate variations in the source mix, calculated using the FLEXPART-COSMO model.

The high-resolution isotope ratio measurements at Cabauw were compared to model calculations that used two different emission inventories. When two very different models (TM5 and FLEXPART-COSMO) used emissions from the EDGAR inventory, they produced clearly too enriched mean isotopic signatures. The modeled mean isotopic signatures were systematically more depleted and closer to the measured ones when the TNO-MACC inventory was used. The differences in the source signatures appear to originate from differences in the inventories and not from differences in the models, which supports indications in the recent literature that fossil fuel related emissions might be overestimated in EDGAR. We note that measurements at Cabauw reflect only one limited region of the European domain, and given the many degrees of freedom (transport, source signatures used in the models, emission inventories), one single dataset is not sufficient to make a final decision on the quality of the emission dataset. High frequency analysis of  $\delta^{13}\text{C}$ - and  $\delta\text{D}$  at several locations would allow better constraints on isotope source signatures and emissions in atmospheric models. Our proof-of-concept study presented here using continuous high-resolution techniques shows that this will be feasible in the future.

## Acknowledgements

This project was funded by the European Community's Seventh Framework Program (FP7/2007-2013) within the InGOS project under grant agreement No. 284274. Additional funding from the Swiss National Science Foundation (SNSF) within grant No. 200021\_134611 and TNA grants within INGOS is gratefully acknowledged. The campaign at the Cabauw tall tower was made possible with strong support from Marcel Brinkenberg (KNMI), Michel Bolder and Henk Snellen (IMAU). We also thank Marco Weber (Empa) for assistance during transport and setup of the TREX-QCLAS system at the CESAR site.

#### **Author contributions**

S.E. and C.vdV. carried out the isotope measurements at the Cabauw tower. C.vdV., T.R. and W.A.B. developed the IRMS system. S.E., B.T., L.E. and J.M. developed the TREX-QCLAS system. C.vdV., S.E., J.M., T.R., B.T., M.E.P., G.Z., D.L., E.G.N., and J.M.N. contributed to the Cabauw measurement campaign. G.M., S.H. and D.B. performed the modeling with TM5 and FLEXPART-COSMO. S.E., T.R., J.M., B.T., E.H., D.B., G.M., S.H., C.vdV., M.E.P. and H.F. performed and contributed to the data evaluation. S.E. produced the figures for the manuscript. T.R., S.E. and J.M. wrote the manuscript with input from C.vdV., G.M., S.H., E.H., D.B., H.F. and L.E. T.R., L.E. and J.M. designed the study as part of the INGOS project.

**Table 1** European CH<sub>4</sub> emissions and isotope source signatures ( $\delta^{13}\text{C}$ ,  $\delta\text{D}$ ) for the different source categories used in TM5.

Process	Yearly emissions (Europe, Tg CH <sub>4</sub> /yr)	source signature $\delta^{13}\text{C}/\text{‰}$
<b>Natural emissions</b>	<b>22.1</b>	<b>-59.2</b>
Natural wetlands (1)		
<i>Peatland</i>	9.3	-68
<i>Wet mineral soils</i>	4.6	-65
<i>Inundated wetlands</i>	1.3	-60
Geological emissions (2)	6.5	-42
Termites (3)	0.4	-63
<b>Anthropogenic emissions</b>	<b>45.3</b>	<b>-52.4</b>
Biomass burning (4)	0,3	-23.6
Agriculture (5)		
<i>Domestic ruminants</i>	11	-64
<i>Manure</i>	3	-54
<i>Rice paddies</i>	0.17	-65
Energy sector (5)		
<i>Coal mining</i>	3.4	-47
<i>Oil production</i>	3	-42
<i>Gas production and distribution</i>	12	-42
<i>Oil combustion</i>	0.41	-32
Residential sector (5)	1.6	-32
Waste treatment (5)		
<i>Landfills</i>	9	-54
<i>Waste waters</i>	3	-50
<b>Total</b>	<b>67.4</b>	<b>-54.6</b>

(1) Spahni et al. (2011); (2) Etiope et al. (2008); (3) Sanderson et al. (1996); (4) GFED3/4 (<http://www.globalfiredata.org/>); (5) EDGAR4.2FT (EDGAR, 2010).

**Table 2** SNAP (Standardized Nomenclature for Air Pollutants) source categories and corresponding  $\delta^{13}\text{C}$  and  $\delta\text{D}$  source signatures from the TNO-MACC\_2 inventory as used in FLEXPART-COSMO.

SNAP Category	Description	$\delta^{13}\text{C}/\text{‰}$	$\delta\text{D}/\text{‰}$
1	Energy industries, oil or gas production	-42	-175
2	Residential combustion	-32	-175
3+4	Industrial combustion and non-combustion processes	-60	-175
5	Extraction and distribution of fossil fuels including distribution of natural gas	-42	-175
7	Road transport	-20	-175
9	Waste including emissions from landfills	-54	-293
10	Agriculture including emissions from ruminants and manure management	-64	-319
6+8	Other emissions (negligible)	-42	-175

739 **Table 3.** Mean value and standard deviation of the histograms of the source  
740 isotopic composition shown in Fig. 10.

Model + Inventory	Method	$\delta^{13}\text{C}/\text{‰}$	$\delta\text{D}/\text{‰}$
Measurement data	MKP	$-61.0 \pm 2.8$	$-300 \pm 22$
TM5 + Edgar	MKP	$-53.3 \pm 1.1$	
FLEXPART-COSMO + Edgar	MKP	$-54.5 \pm 1.6$	$-277 \pm 10$
FLEXPART-COSMO + Edgar	Direct	$-53.4 \pm 1.7$	$-269 \pm 10$
TM5 + TNO-MACC	MKP	$-56.7 \pm 0.8$	
FLEXPART-COSMO + TNO-MACC	MKP	$-57.6 \pm 1.9$	$-294 \pm 12$
FLEXPART-COSMO + TNO-MACC	Direct	$-57.2 \pm 1.7$	$-289 \pm 11$

741

## 742 Figures

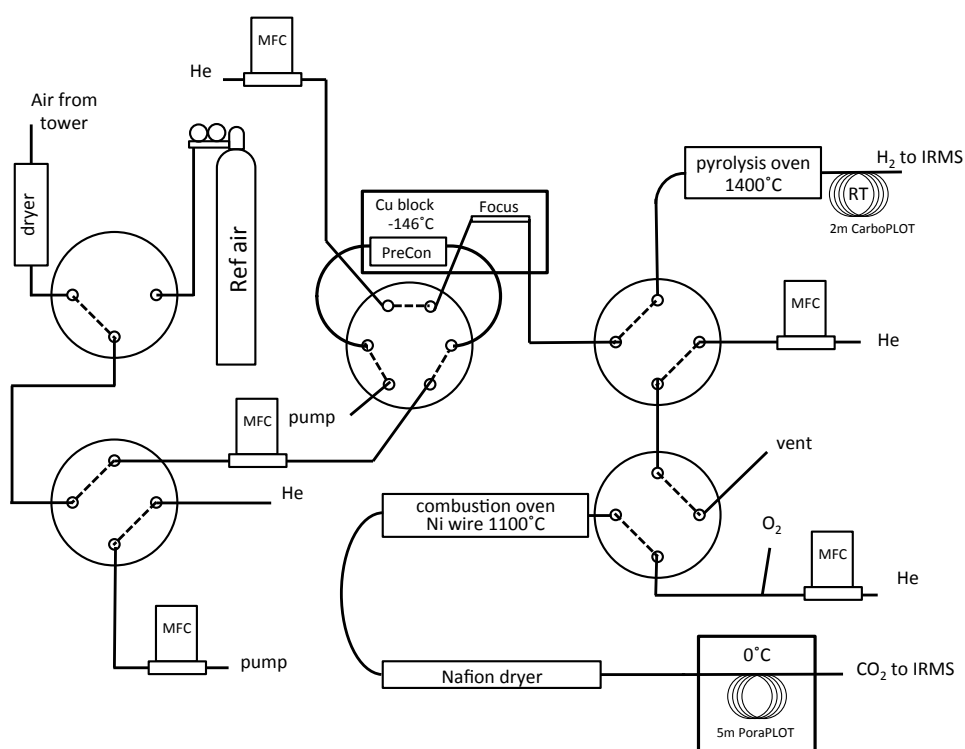


Fig. 1: Schematics of the pre-concentration and extraction system developed for the IRMS technique. MFC denotes mass flow controller. The 8-port valve through which the Ref air bottle was connected to the first selection valve is not shown to reduce complexity. For further description see the main text.



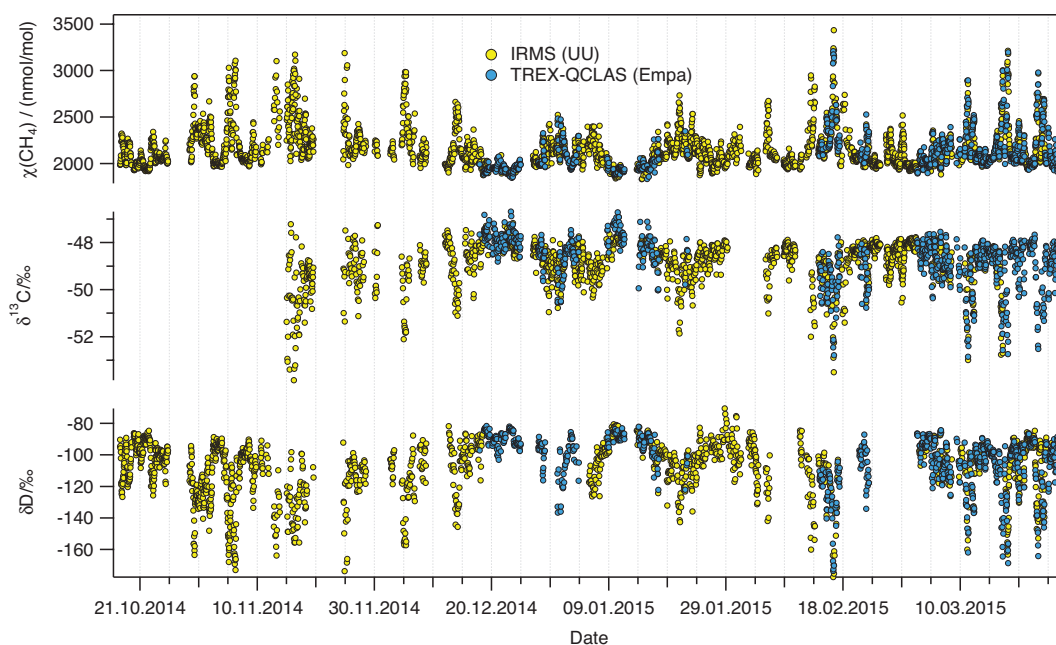
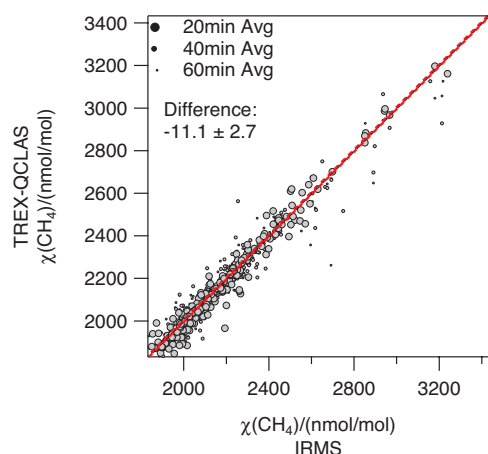
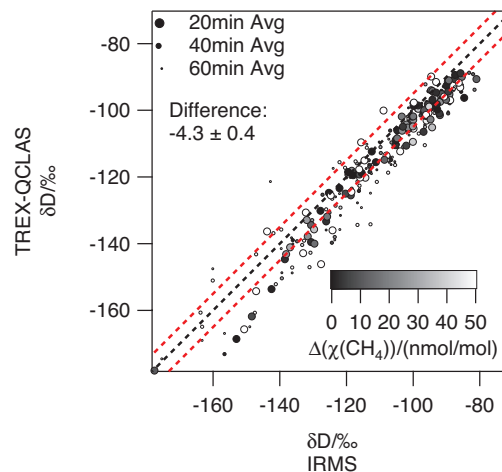
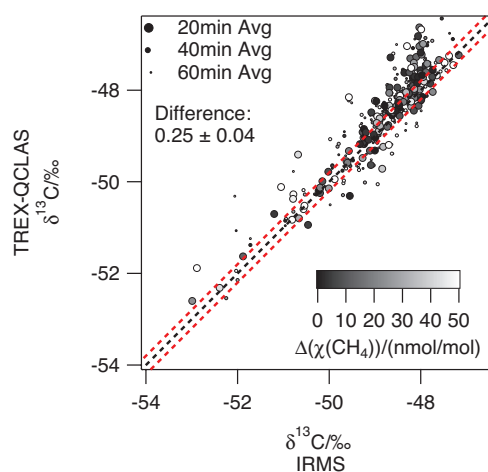


Fig. 2: CH<sub>4</sub> mole fraction,  $\chi(\text{CH}_4)$ , and isotopic composition ( $\delta^{13}\text{C}$ ,  $\delta\text{D}$ ) measured at the Cabauw tall tower from 17 October 2014 until 29 March 2015. Real-time measurements by IRMS (Utrecht University) are indicated in yellow, TREX-QCLAS (Empa) data in blue.

756



757



758

759

760

761 Fig. 3: Correlation diagrams for CH<sub>4</sub> mole fraction, δ<sup>13</sup>C and δD analyzed with  
 762 IRMS (Utrecht University) and TREX-QCLAS (Empa). The dashed black lines are  
 763 1:1 lines, dashed red lines mark the extended WMO compatibility goals of ± 5  
 764 nmol/mol, ± 0.2 ‰ and ± 5 ‰ for CH<sub>4</sub> mole fraction, δ<sup>13</sup>C and δD, respectively.  
 765 The temporal difference between IRMS and TREX-QCLAS sampling is indicated  
 766 by the point size (large: 20 min, medium: 40 min, small: 60 min). For δ<sup>13</sup>C and δD,  
 767 the differences in the CH<sub>4</sub> mole fraction of the measurements are represented by  
 768 the shading (black: identical mole fractions, white: 50 nmol/mol difference).

769

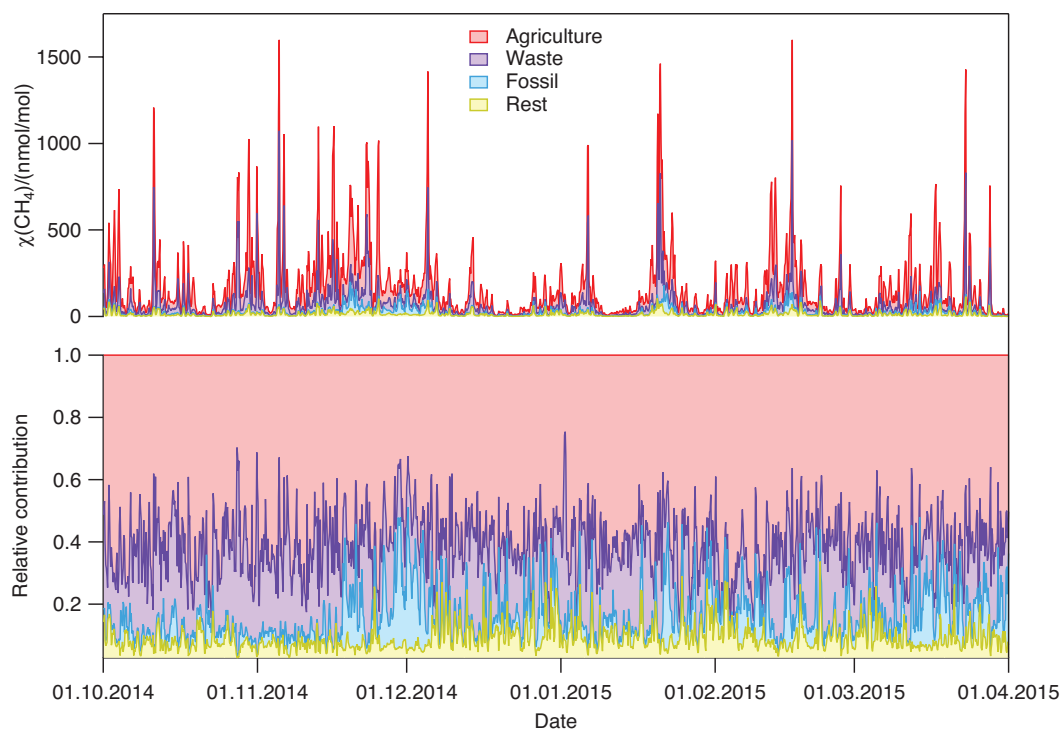


Fig. 4: Absolute (top) and relative (bottom) contributions of methane emissions that are picked up along the 4-day FLEXPART-COSMO trajectories during the campaign. The results shown are from the FLEXPART-COSMO simulations with the TNO-MACC inventory. They indicate major contributions of the following source categories: “agriculture” (mainly ruminants), “waste” (mainly landfills) and “fossil” (fugitive losses from coal, oil and natural gas production and from gas transportation and distribution) to the increase in  $\text{CH}_4$  mole fractions at Cabauw. The category “rest” primarily represents residential  $\text{CH}_4$  emissions.

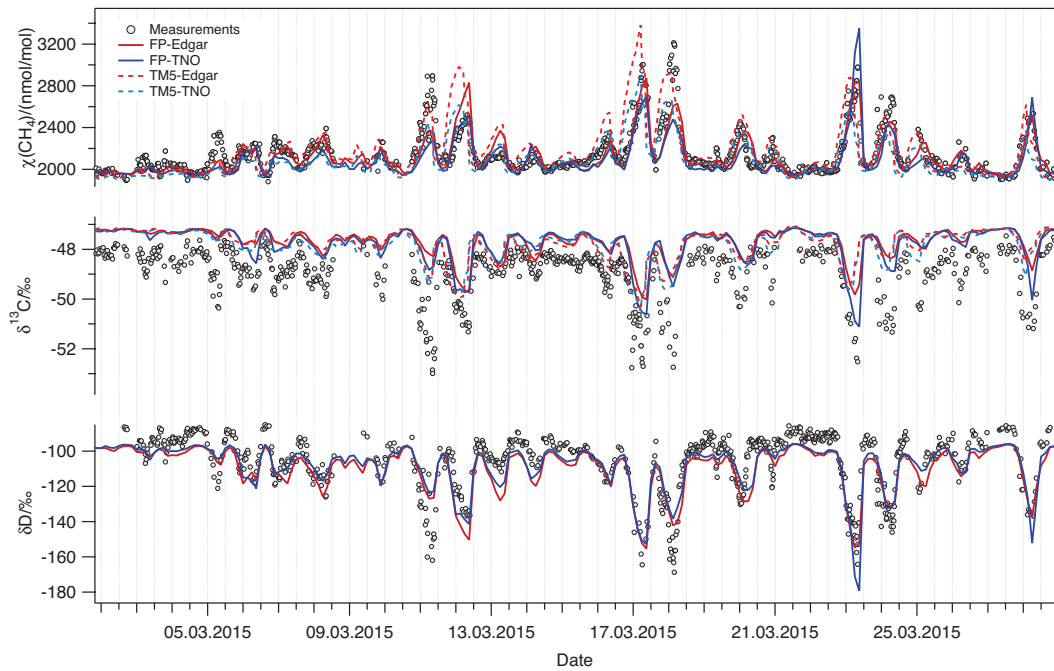
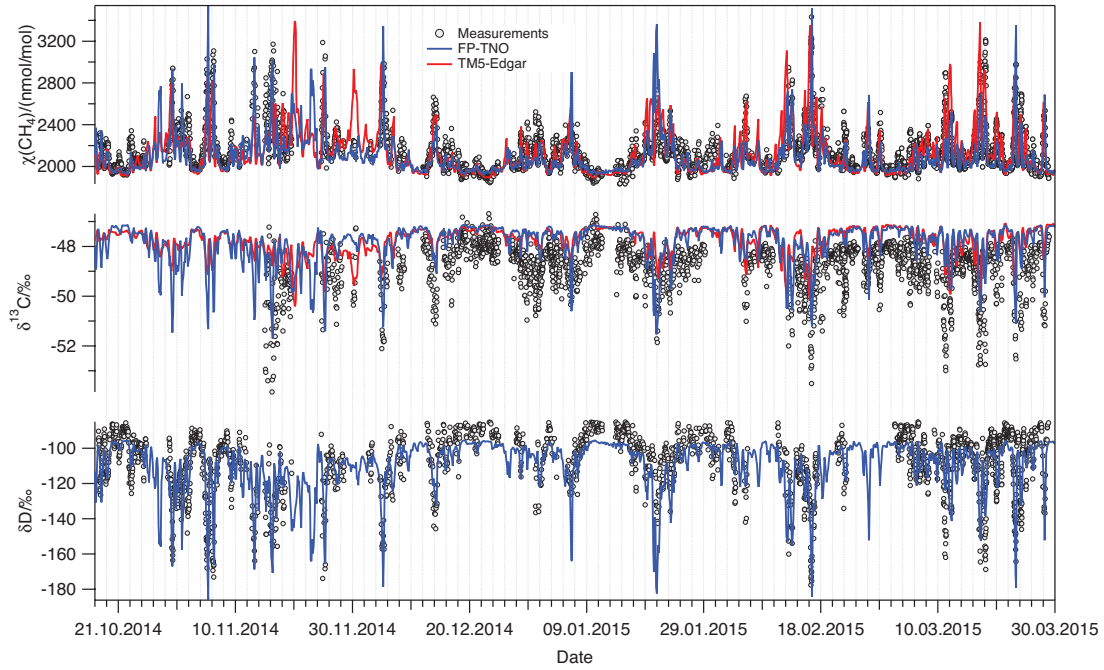


Fig. 5: Comparison of the modeled and measured time series of  $\text{CH}_4$  mole fraction and isotopic composition ( $\delta^{13}\text{C}$ - and  $\delta\text{D}$ ). Measurements are shown as circles and model results as lines. Top graph: two selected model configurations for the entire campaign: FLEXPART-COSMO using the TNO-MACC inventory (blue) and TM5 using the Edgar/Why-Me inventory (red). Bottom graph: Time series for March 2015 with all four model – inventory combinations. For  $\delta\text{D}$ , only the synthetic FLEXPART-COSMO results are available for comparison since TM5 does not simulate  $\delta\text{D}$ .

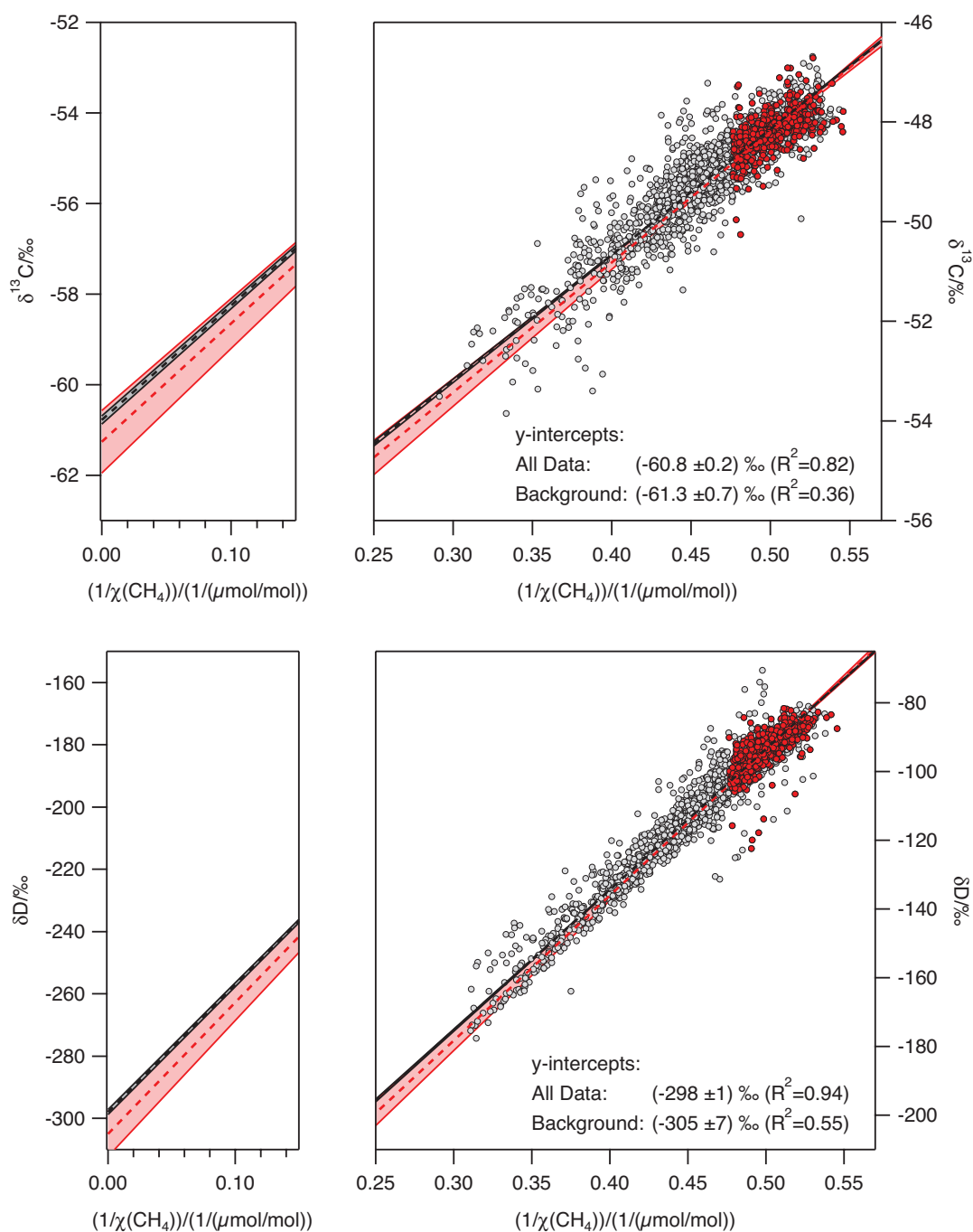
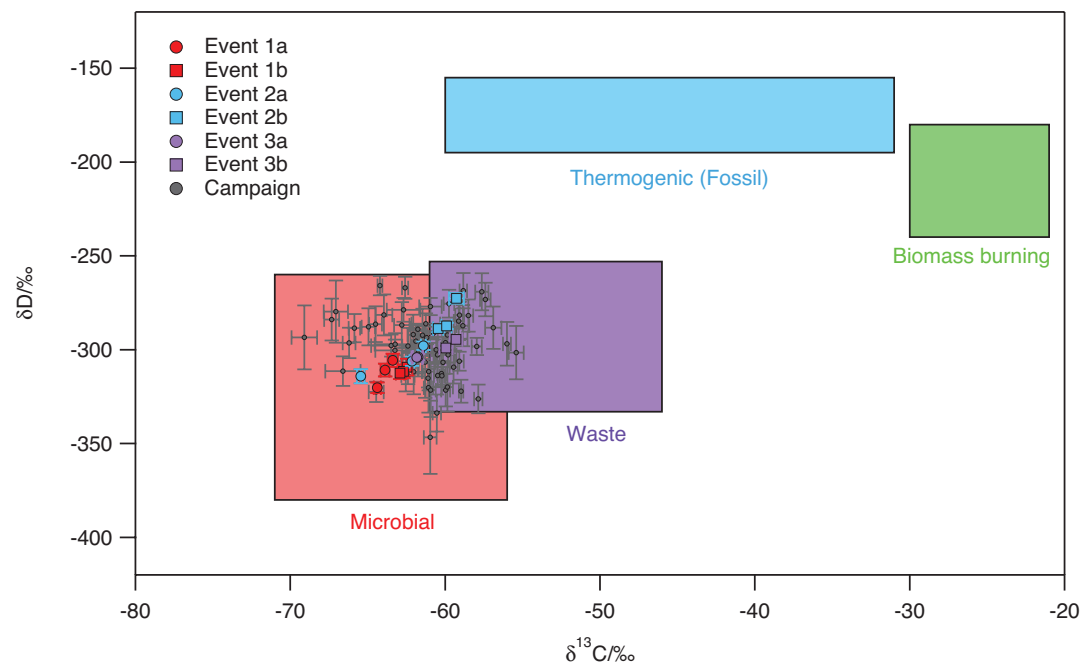


Fig. 6: Keeling plot of all data using an orthogonal regression method. The dashed line indicates the regression line and the shaded area the confidence interval taking into account the measurement uncertainties. The color code indicates all measured data (grey points) and daily background values (red points). Left panels show the region near the y-axis intercept.



799

800

801

802

803

804

805

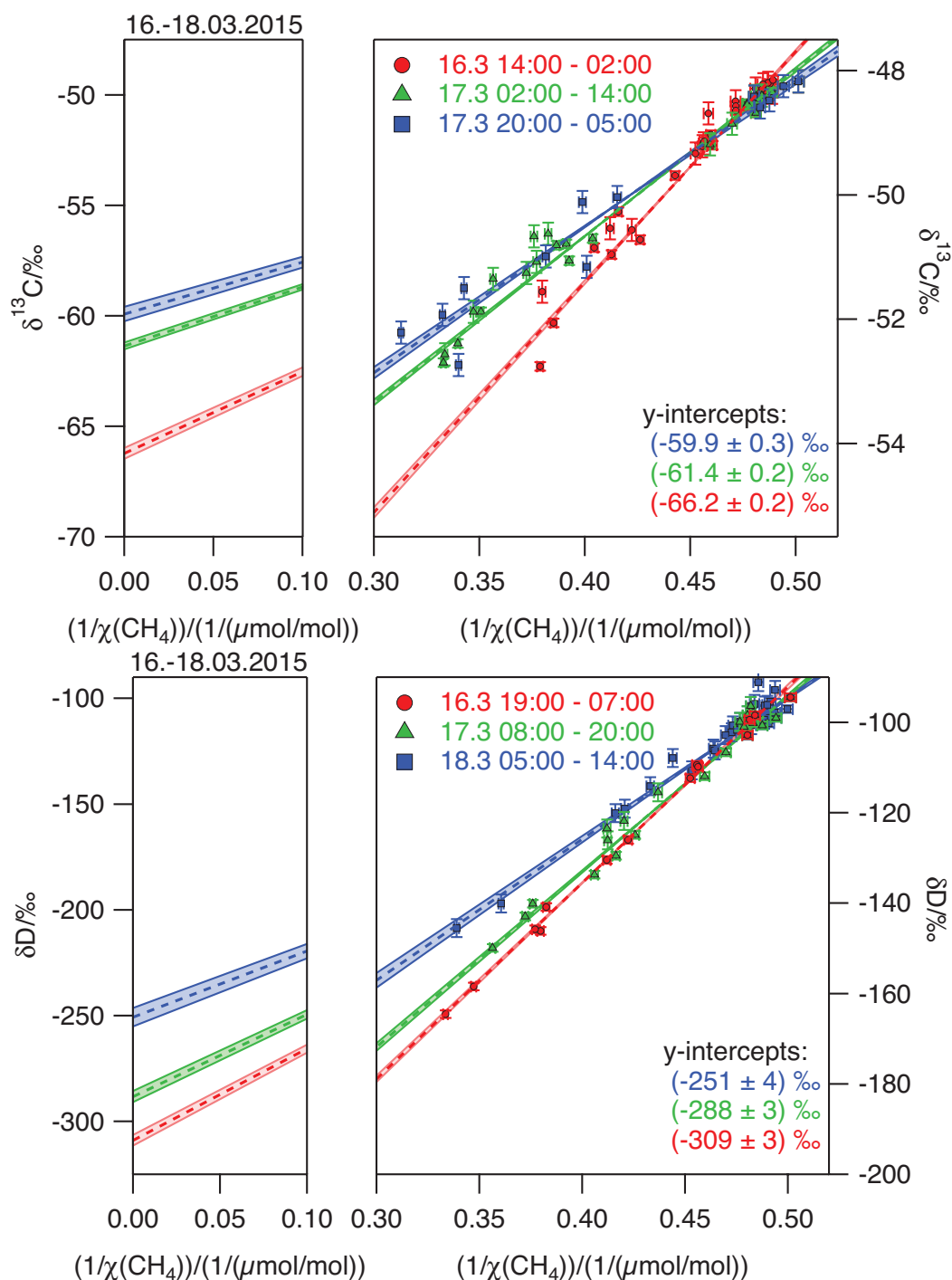
806

807

808

809

Fig. 7: MKP intercepts of  $\delta D$  vs.  $\delta^{13}C$ . The colored areas indicate typical isotope signatures for different source categories. Circles show the 6h-averaged source signatures. Large colored symbols indicate data from the three events (event 1: 10<sup>th</sup> – 12<sup>th</sup> March, event 2: 16<sup>th</sup> – 18<sup>th</sup> March, event 3: 22<sup>nd</sup> to 24<sup>th</sup> March) that are highlighted in Fig. 9. The labels a and b refer to day 1 and day 2 of the two-day events, respectively. For the source signatures, the  $\delta^{13}C$  values are taken from Table 1 and the  $\delta D$  values from recent literature (Snover et al., 2000; Rigby et al., 2012).



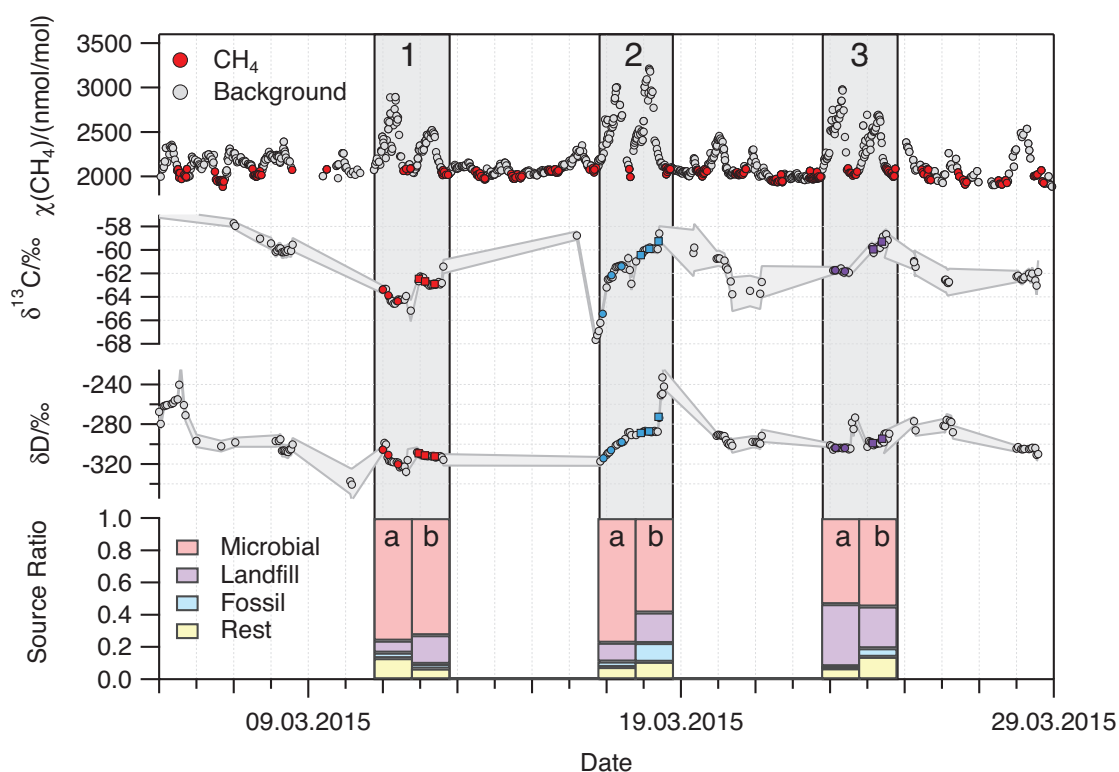
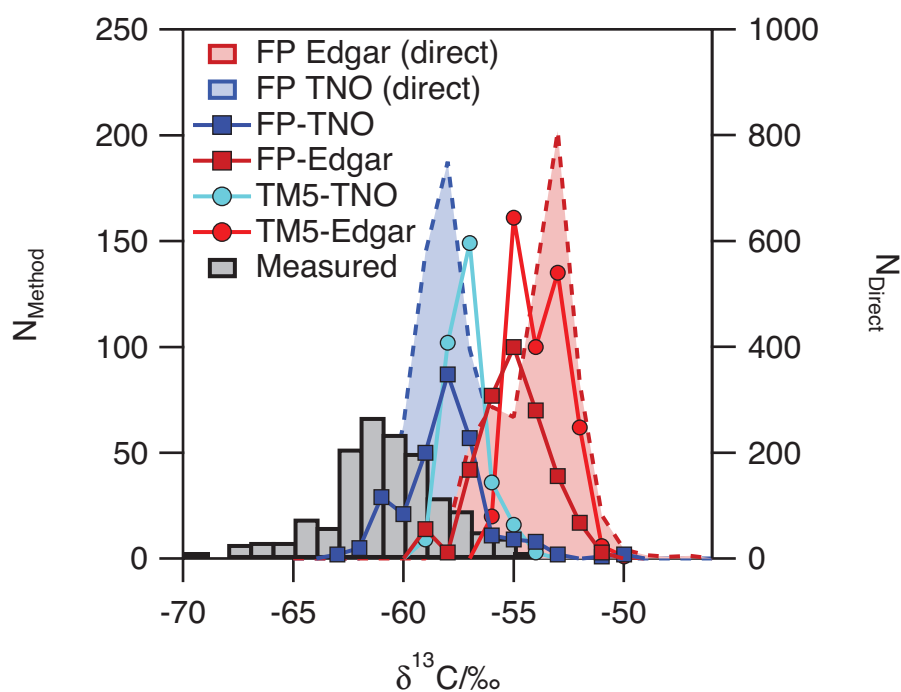


Fig. 9: Detailed analysis of three 2-day periods with large CH<sub>4</sub> elevations in March 2015. The top panel exhibits CH<sub>4</sub> mole fraction (grey) with background values in red (10:00-18:00, >2100 nmol/mol). The middle panels show the mean isotopic signatures ( $\delta^{13}\text{C}$ ,  $\delta\text{D}$ ) derived with the 12-h MKP method. The color-coding in the middle panels (red, light blue, purple) indicates characteristic contributions from different sources; red-microbial, light blue-fossil, purple-waste. For consistency, the same color-coding was chosen in Fig. 7. The bottom graph presents CH<sub>4</sub> source contributions as computed with the FLEXPART-COSMO model using the TNO-MACC inventory, averaged over 24 hours.

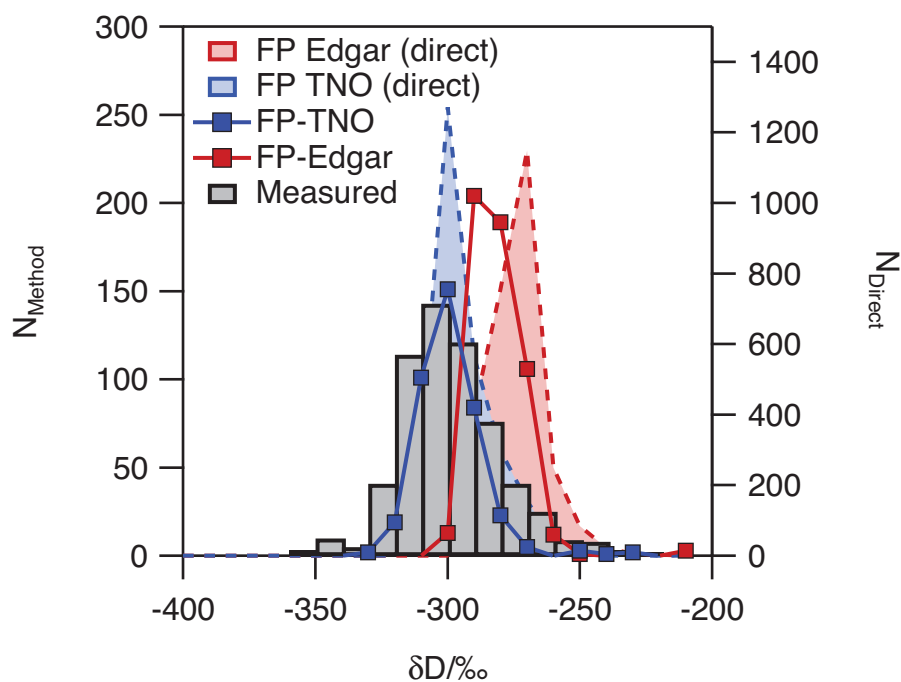


838

839



840



841

842 Fig. 10: Histograms of CH<sub>4</sub> isotope source signatures at the CESAR site between  
 843 October 2014 and March 2015. Bin widths are 1 ‰ for  $\delta^{13}\text{C}$  and 10 ‰ for  $\delta\text{D}$ .  
 844 **Mean isotopic signatures** are derived from measured data (grey bins),  
 845 FLEXPART-COSMO modeling (squares) as well as TM5 modeling (circles) using  
 846 the 12 h MKP method. Two different inventories, TNO-MACC (blue) and

847 Edgar/LPJ-Why-Me (red), were used. The shaded areas show histograms for the  
848 “direct” source signatures that were picked up along the FLEXPART-COSMO  
849 trajectory (right axis).

## 850 References

- 851 Baertschi, P.: Absolute  $^{18}\text{O}$  content of Standard Mean Ocean Water, *Earth*  
852 *Planet. Sci. Lett.*, 31, 341-344, 1976.
- 853 Baldauf, M., Seifert, A., Förstner, J., Majewski, D., Raschendorfer, M., and  
854 Reinhardt, T.: Operational Convective-Scale Numerical Weather Prediction with the  
855 COSMO Model: Description and Sensitivities, *Monthly Weather Review*, 139, 3887–  
856 3905, doi:3810.1175/MWR-D-3810-05013.05011, 2011.
- 857 Beck, V., Chen, H. L., Gerbig, C., Bergamaschi, P., Bruhwiler, L., Houweling, S.,  
858 Röckmann, T., Kolle, O., Steinbach, J., Koch, T., Sapart, C. J., van der Veen, C.,  
859 Frankenberg, C., Andreae, M. O., Artaxo, P., Longo, K. M., and Wofsy, S. C.:  
860 Methane airborne measurements and comparison to global models during BARCA, *J.*  
861 *Geophys. Res.*, 117, D15310, doi:15310.11029/12011JD017345, 2012.
- 862 Bergamaschi, P., Brenninkmeijer, C. A. M., Hahn, M., Röckmann, T., Scharffe,  
863 D. H., Crutzen, P. J., Elansky, N. F., Belikov, I. B., Trivett, N. B. A., and Worthy, D.  
864 E. J.: Isotope analysis based source identification for atmospheric  $\text{CH}_4$  and  $\text{CO}$  across  
865 Russia using the Trans-Siberian railroad, *J. Geophys. Res.*, 103, D7, 8227-8235, DOI:  
866 8210.1029/8297JD03738, 1998a.
- 867 Bergamaschi, P., Houweling, S., Segers, A., Krol, M., Frankenberg, C.,  
868 Scheepmaker, R. A., Dlugokencky, E., Wofsy, S. C., Kort, E. A., Sweeney, C.,  
869 Schuck, T., Brenninkmeijer, C., Chen, H., Beck, V., and Gerbig, C.: Atmospheric  
870  $\text{CH}_4$  in the first decade of the 21st century: Inverse modeling analysis using  
871 SCIAMACHY satellite retrievals and NOAA surface measurements, *J Geophys Res-*  
872 *Atmos*, 118, 7350–7369, doi:7310.1002/jgrd.50480, 2013.
- 873 Bergamaschi, P., Lubina, C., Konigstedt, R., Fischer, H., Veltkamp, A. C., and  
874 Zwaagstra, O.: Stable isotopic signatures ( $\delta^{13}\text{C}$ ,  $\delta\text{D}$ ) of methane from European  
875 landfill sites, *J. Geophys. Res.*, 103, 8251-8265, doi 8210.1029/8298jd00105, 1998b.
- 876 Bergamaschi, P., Schupp, M., and Harris, G. W.: High-precision direct  
877 measurements of  $^{13}\text{CH}_4/^{12}\text{CH}_4$  and  $\text{CH}_3\text{D}/^{12}\text{CH}_4$  ratios in atmospheric methane  
878 sources by means of a long-path tunable diode laser absorption spectrometer, *Appl.*  
879 *Opt.*, 33, No.33, 7704-7716, 1994.
- 880 Bock, M., Schmitt, J., Behrens, M., Moller, L., Schneider, R., Sapart, C., and  
881 Fischer, H.: A gas chromatography/pyrolysis/isotope ratio mass spectrometry system  
882 for high-precision  $\delta\text{D}$  measurements of atmospheric methane extracted from ice cores,  
883 *Rap. Commun. Mass Spectrom.*, 24, 621-633, 2010.
- 884 Brass, M. and Röckmann, T.: Continuous-flow isotope ratio mass spectrometry  
885 method for carbon and hydrogen isotope measurements on atmospheric methane,  
886 *Atmos. Meas. Tech.*, 3, 1707-1721, 2010.
- 887 Brenninkmeijer, C. A. M., Lowe, D. C., Manning, M. R., Sparks, R. J., and  
888 Velthoven, P. F. J. v.: The  $^{13}\text{C}$ ,  $^{14}\text{C}$ , and  $^{18}\text{O}$  isotopic composition of  $\text{CO}$ ,  $\text{CH}_4$  and  
889  $\text{CO}_2$  in the higher southern latitudes lower stratosphere, *J. Geophys. Res.*, 100,  
890 26,163-126,172, 1995.

891 Bruhwiler, L., Dlugokencky, E., Masarie, K., Ishizawa, M., Andrews, A., Miller,  
892 J., Sweeney, C., Tans, P., and Worthy, D.: CarbonTracker-CH<sub>4</sub>: an assimilation  
893 system for estimating emissions of atmospheric methane, *Atmos. Chem. Phys.*, 14,  
894 8269-8293, 2014.

895 Craig, H.: Isotopic standards for carbon and oxygen and correction factors for  
896 mass-spectrometric analysis of carbon dioxide, *Geochim. Cosmochim. Acta*, 12, 133-  
897 149, 1957.

898 Dee, D. P., Uppala, S. M., Simmons, A. J., Berrisford, P., Poli, P., and al., e.: The  
899 ERA-Interim reanalysis: configuration and performance of the data assimilation  
900 system, *Quart. J. Roy. Meteor. Soc.*, 553-579, 2011.

901 Dlugokencky, E. J., Bruhwiler, L., White, J. W. C., Emmons, L. K., Novelli, P.  
902 C., Montzka, S. A., Masarie, K. A., Lang, P. M., Crotwell, A. M., Miller, J. B., and  
903 Gatti, L. V.: Observational constraints on recent increases in the atmospheric CH<sub>4</sub>  
904 burden, *Geophys. Res. Lett.*, 36, L18803, doi 10.1029/2009gl039780, 2009.

905 Dlugokencky, E. J., Dutton, E. G., Novelli, P. C., Tans, P. P., Masarie, K. A.,  
906 Lantz, K. O., and Madronich, S.: Changes in CH<sub>4</sub> and CO growth rates after the  
907 eruption of Mt. Pinatubo and their link with changes in tropical tropospheric UV flux,  
908 *Geophys. Res. Lett.*, 23, 2761-2764, 1996.

909 Dlugokencky, E. J., Masarie, K. A., Lang, P. M., and Tans, P. P.: Continuing  
910 decline in the growth rate of the atmospheric methane burden, *Nature*, 393, 447-450,  
911 1998.

912 Dlugokencky, E. J., Myers, R. C., Lang, P. M., Masarie, K. A., Crotwell, A. M.,  
913 Thoning, K. W., Hall, B. D., Elkins, J. W., and Steele, L. P.: Conversion of NOAA  
914 atmospheric dry air CH<sub>4</sub> mole fractions to a gravimetrically prepared standard scale, *J.*  
915 *Geophys. Res.*, 110, D18306, Doi 10.1029/2005jd006035, 2005.

916 EDGAR: European Commission, Joint Research Centre (JRC)/Netherlands  
917 Environmental Assessment Agency (PBL). , Emission Database for Global  
918 Atmospheric Research (EDGAR), Version 4.2. , 2010. Available at  
919 <http://edgar.jrc.ec.europa.eu>, 2010.

920 EDGAR: European Commission, Joint Research Centre (JRC)/Netherlands  
921 Environmental Assessment Agency (PBL). Emission Database for Global  
922 Atmospheric Research (EDGAR), release version 4.2.  
923 <http://edgar.jrc.ec.europa.eu>, 2009.

924 Etheridge, D. M., Steele, L. P., Francey, R. J., and Langenfelds, R. L.:  
925 Atmospheric methane between 1000 AD and present: Evidence of antropogenic  
926 emissions and climatic variability, *J. Geophys. Res.*, 103, 15979-15993, 1998.

927 Etiope, G., Lassey, K. R., Klusman, R. W., and Boschi, E.: Reappraisal of the  
928 fossil methane budget and related emission from geologic sources, *Geophys. Res.*  
929 *Lett.*, 35, 2008.

930 Eyer, S. and al, e.: Real-time analysis of  $\delta^{13}\text{C}$ - and  $\delta\text{D}$ -CH<sub>4</sub> in ambient air with  
931 laser spectroscopy: Method development and first intercomparison results., *Atmos.*  
932 *Meas. Tech. Discuss.*, 8, 8925-8970, 2015.

933 Eyer, S., Stadie, N. P., Borgschulte, A., Emmenegger, L., and Mohn, J.: Methane  
934 preconcentration by adsorption: a methodology for materials and conditions selection,  
935 *Adsorption-Journal of the International Adsorption Society*, 20, 657-666, 2014.

936 Ferretti, D., Miller, J., White, J., Etheridge, D., Lassey, K., Lowe, D., Allan, B.,  
 937 MacFarling, C., Dreier, M., Trudinger, C., and Ommen, T. v.: Unexpected changes to  
 938 the global methane budget over the past 2000 years, *Science*, 309, 1714-1717, 2005.

939 Fischer, H., Behrens, M., Bock, M., Richter, U., Schmitt, J., Loulergue, L.,  
 940 Chappellaz, J., Spahni, R., Blunier, T., Leuenberger, M., and Stocker, T. F.: Changing  
 941 boreal methane sources and constant biomass burning during the last termination,  
 942 *Nature*, 452, 864-867, 2008.

943 Gros, V., Brenninkmeijer, C. A. M., Jöckel, P., Kaiser, J., Lowry, D., Nisbet, E.  
 944 G., O'Brian, P., Röckmann, T., and Warwick, N.: Isotope signatures of trace gas  
 945 sources. In: *Emissions Of Atmospheric Trace Compounds*, Granier, C., Artaxo, P.,  
 946 and Reeves, C. E. (Eds.), *Advances in Global Change Research*, Kluwer Academic  
 947 Pub., Paris, 2004.

948 Henne, S., Brunner, D., Oney, B., Leuenberger, M., Eugster, W., Bamberger, I.,  
 949 Meinhardt, F., Steinbacher, M., and Emmenegger, L.: Validation of the Swiss  
 950 methane emission inventory by atmospheric observations and inverse modelling,  
 951 *Atmos. Chem. Phys. Discuss.*, 2015. 35417-35484, doi:35410.35194/acpd-35415-  
 952 35417-32015, 2015.

953 Hiller, R. V., Bretscher, D., DelSontro, T., Diem, T., Eugster, W., Henneberger,  
 954 R., Hobi, S., Hodson, E., Imer, D., Kreuzer, M., Künzle, T., Merbold, L., Niklaus, P.  
 955 A., Rihm, B., Schellenberger, A., Schroth, M. H., Schubert, C. J., Siegrist, H., Stieger,  
 956 J., Buchmann, N., and Brunner, D.: Anthropogenic and natural methane fluxes in  
 957 Switzerland synthesized within a spatially explicit inventory, *Biogeosciences*, 11,  
 958 1941-1959, doi:1910.5194/bg-1911-1941-2014, 2014.

959 Houweling, S., Krol, M., Bergamaschi, P., Frankenberg, C., Dlugokencky, E. J.,  
 960 Morino, I., Notholt, J., Sherlock, V., Wunch, D., Beck, V., Gerbig, C., Chen, H., Kort,  
 961 E. A., Röckmann, T., and Aben, I.: A multi-year methane inversion using  
 962 SCIAMACHY, accounting for systematic errors using TCCON measurements,  
 963 *Atmos. Chem. Phys.*, 14, 3991-4012, 2014.

964 Houweling, S., van der Werf, G. R., Goldewijk, K. K., Röckmann, T., and Aben,  
 965 I.: Early anthropogenic CH<sub>4</sub> emissions and the variation of CH<sub>4</sub> and <sup>13</sup>CH<sub>4</sub> over the  
 966 last millennium, *Global Biogeochem Cy*, 22, 2008.

967 Kawagucci, S., Kobayashi, M., Hattori, S., Yamada, K., Ueno, Y., Takai, K., and  
 968 Yoshida, N.: Hydrogen isotope systematics among H<sub>2</sub>-H<sub>2</sub>O-CH<sub>4</sub> during the growth of  
 969 the hydrogenotrophic methanogen *Methanothermobacter thermautotrophicus* strain  
 970 Delta H, *Geochim Cosmochim Acta*, 142, 601-614, 2014.

971 Keeling, C. D.: The Concentration and Isotopic Abundances of Carbon Dioxide  
 972 in Rural and Marine Air, *Geochim. Cosmochim. Acta*, 24, 277-298, 1961.

973 Khalil, M. A. K., Butenhoff, C. L., and Rasmussen, R. A.: Atmospheric methane:  
 974 Trends and cycles of sources and sinks, *Environmental Science & Technology*, 41,  
 975 2131-2137, 2007.

976 Kirschke, S., Bousquet, P., Ciais, P., Saunois, M., Canadell, J. G., Dlugokencky,  
 977 E. J., Bergamaschi, P., Bergmann, D., Blake, D. R., Bruhwiler, L., Cameron-Smith,  
 978 P., Castaldi, S., Chevallier, F., Feng, L., Fraser, A., Heimann, M., Hodson, E. L.,  
 979 Houweling, S., Josse, B., Fraser, P. J., Krummel, P. B., Lamarque, J. F., Langenfelds,  
 980 R. L., Le Quere, C., Naik, V., O'Doherty, S., Palmer, P. I., Pison, I., Plummer, D.,  
 981 Poulter, B., Prinn, R. G., Rigby, M., Ringeval, B., Santini, M., Schmidt, M., Shindell,  
 982 D. T., Simpson, I. J., Spahni, R., Steele, L. P., Strode, S. A., Sudo, K., Szopa, S., van  
 983 der Werf, G. R., Voulgarakis, A., van Weele, M., Weiss, R. F., Williams, J. E., and

984 Zeng, G.: Three decades of global methane sources and sinks, *Nat Geosci*, 6, 813-823,  
985 2013.

986 Klevenhusen, F., Bernasconi, S. M., Kreuzer, M., and Soliva, C. R.: Experimental  
987 validation of the Intergovernmental Panel on Climate Change default values for  
988 ruminant-derived methane and its carbon-isotope signature, *Anim Prod Sci*, 50, 159-  
989 167, 2010.

990 Krol, M., Houweling, S., Bregman, B., van den Broek, M., Segers, A., van  
991 Velthoven, P., Peters, W., Dentener, F., and Bergamaschi, P.: The two-way nested  
992 global chemistry-transport zoom model TM5: algorithm and applications, *Atmos.*  
993 *Chem. Phys.*, 5, 417-432, 2005.

994 Kuenen, J. J. P., Visschedijk, A. J. H., Jozwicka, M., and van der Gon, H. A. C.  
995 D.: TNO-MACC-II emission inventory; a multi-year (2003-2009) consistent high-  
996 resolution European emission inventory for air quality modelling, *Atmos. Chem.*  
997 *Phys.*, 14, 10963-10976, 2014.

998 Lassey, K. R., Lowe, D. C., Brenninkmeijer, C. A. M., and Gomez, A. J.:  
999 Atmospheric Methane and its Carbon Isotopes in the Southern Hemisphere: their  
1000 Time Series and an Instructive Model, *Chemosphere*, 26, 95-109, 1993.

1001 Lassey, K. R., Lowe, D. C., and Manning, M. R.: The trend in atmospheric  
1002 methane  $\delta^{13}\text{C}$  implications for isotopic constraints on the global methane budget,  
1003 *Global Biogeochem Cy*, 14, 41-49, 2000.

1004 Louergue, L., Schilt, A., Spahni, R., Masson-Delmotte, V., Blunier, T., Lemieux,  
1005 B., Barnola, J. M., Raynaud, D., Stocker, T. F., and Chappellaz, J.: Orbital and  
1006 millennial-scale features of atmospheric  $\text{CH}_4$  over the past 800,000 years, *Nature*,  
1007 453, 383-386, 2008.

1008 Lowe, D. C., Brenninkmeijer, C. A. M., Brailsford, G. W., Lassey, K. R., Gomez,  
1009 A. J., and Nisbet, E. G.: Concentration and  $^{13}\text{C}$  Records of Atmospheric Methane in  
1010 New-Zealand and Antarctica - Evidence for Changes in Methane Sources, *J. Geophys.*  
1011 *Res.*, 99, 16913-16925, 1994.

1012 MacFarling Meure, C., Etheridge, D., Trudinger, C., Steele, P., Langenfelds, R.,  
1013 Ommen, T. v., Smith, A., and Elkins, J.: Law Dome  $\text{CO}_2$ ,  $\text{CH}_4$  and  $\text{N}_2\text{O}$  ice core  
1014 records extended to 2000 years BP *Geophys. Res. Lett.*, 33, L14810,  
1015 doi:14810.11029/12006GL026152 2006.

1016 Merritt, D. A., Brand, W. A., and Hayes, J. M.: Isotope-ratio-monitoring gas  
1017 chromatography-mass spectrometry: methods for isotopic calibration, *Org. Geochem.*,  
1018 21 No. 6/7, 573-583, 1994.

1019 Merritt, D. A., Hayes, J. M., and Des Marais, D. J.: Carbon isotopic analysis of  
1020 atmospheric methane by isotope-ratio-monitoring gas chromatography-mass  
1021 spectrometry, *J. Geophys. Res.*, 100 D, 1317-1326, 1995.

1022 Mohn, J., Guggenheim, C., Tuzson, B., Vollmer, M. K., Toyoda, S., Yoshida, N.,  
1023 and Emmenegger, L.: A liquid nitrogen-free preconcentration unit for measurements  
1024 of ambient  $\text{N}_2\text{O}$  isotopomers by QCLAS, *Atmos Meas Tech*, 3, 609-618, 2010.

1025 Mohn, J., Tuzson, B., Manninen, A., Yoshida, N., Toyoda, S., Brand, W. A., and  
1026 Emmenegger, L.: Site selective real-time measurements of atmospheric  $\text{N}_2\text{O}$   
1027 isotopomers by laser spectroscopy, *Atmos Meas Tech*, 5, 1601-1609, 2012.

1028 Monteil, G., Houweling, S., Dlugockenky, E. J., Maenhout, G., Vaughn, B. H.,  
1029 White, J. W. C., and Röckmann, T.: Interpreting methane variations in the past two

decades using measurements of CH<sub>4</sub> mixing ratio and isotopic composition, *Atmos. Chem. Phys.*, 11, 9141-9153, 2011.

Monteil, G., Houweling, S., Guerlet, S., Schepers, D., Frankenberg, C., Scheepmaker, R., Aben, I., Butz, A., Hasekamp, O., Landgraf, J., Wofsy, S. C., and Röckmann, T.: Intercomparison of 15 months inversions of GOSAT and SCIAMACHY CH<sub>4</sub> retrievals, *J. Geophys. Res.*, 118, 11807-11823, doi:10.1029/2013JD019760, 2013.

Nisbet, E. G., Dlugokencky, E. J., and Bousquet, P.: Methane on the rise—again, *Science*, 343, 493-495, 2014.

Pataki, D. E., Ehleringer, J. R., Flanagan, L. B., Yakir, D., Bowling, D. R., Still, C. J., Buchmann, N., Kaplan, J. O., and Berry, J. A.: The application and interpretation of Keeling plots in terrestrial carbon cycle research, *Global Biogeochem Cy*, 17, 1022, doi:10.1029/2001GB001850, 2003.

Peltola, O., Hensen, A., Helfter, C., Marchesini, L. B., Bosveld, F. C., van den Bulk, W. C. M., Elbers, J. A., Haapanala, S., Holst, J., Laurila, T., Lindroth, A., Nemitz, E., Röckmann, T., Vermeulen, A. T., and Mammarella, I.: Evaluating the performance of commonly used gas analysers for methane eddy covariance flux measurements: the InGOS inter-comparison field experiment, *Biogeosciences*, 11, 3163-3186, 2014.

Peltola, O., Hensen, A., Marchesini, L. B., Helfter, C., Bosveld, F. C., van den Bulk, W. C. M., Haapanala, S., van Huissteden, J., Laurila, T., Lindroth, A., Nemitz, E., Röckmann, T., Vermeulen, A. T., and Mammarella, I.: Studying the spatial variability of methane flux with five eddy covariance towers of varying height, *Agricultural and Forest Meteorology*, 214, 456-472, 2015.

Quay, P., Stutsman, J., Wilbur, D., Snover, A., Dlugokencky, E., and Brown, T.: The isotopic composition of atmospheric methane, *Global Biogeochem Cy*, 13, 445-461, 1999.

Rasmussen, R. A. and Khalil, M. A. K.: Atmospheric Methane (CH<sub>4</sub>) - Trends and Seasonal Cycles, *J. Geophys. Res.*, 86, 9826-9832, 1981.

Rigby, M., Manning, A. J., and Prinn, R. G.: The value of high-frequency, high-precision methane isotopologue measurements for source and sink estimation, *J. Geophys. Res.*, 117, 2012.

Röckmann, T., Brass, M., Borchers, R., and Engel, A.: The isotopic composition of methane in the stratosphere: High-altitude balloon sample measurements, *Atm. Chem. Phys.*, 11, 13287-13304, 2011.

Sanderson, M. G.: Biomass of termites and their emissions of methane and carbon dioxide: A global database, *Global Biogeochem. Cycles*, 10, 543-557, 1996.

Sapart, C. J., Monteil, G., Prokopiou, M., van de Wal, R. S. W., Kaplan, J. O., Sperlich, P., Krumhardt, K. M., van der Veen, C., Houweling, S., Krol, M. C., Blunier, T., Sowers, T., Martinerie, P., Witrant, E., Dahl-Jensen, D., and Röckmann, T.: Natural and anthropogenic variations in methane sources during the past two millennia, *Nature*, 490, 85-88, 2012.

Sapart, C. J., Veen, C. v. d., Vigano, I., Brass, M., Wal, R. S. W. v. d., Bock, M., Fischer, H., Sowers, T., Buizert, C., Sperlich, P., Blunier, T., Behrens, M., Schmitt, J., Seth, B., and Röckmann, T.: Simultaneous stable isotope analysis of methane and nitrous oxide on ice core samples, *Atmos. Meas. Tech.*, 4, 2607-2618, 2011.

1076 Saueressig, G., Bergamaschi, P., Crowley, J. N., Fischer, H., and Harris, G. W.:  
 1077 D/H kinetic isotope effect in the reaction  $\text{CH}_4 + \text{Cl}$ , *Geophys. Res. Lett.*, 23, 3619-  
 1078 3622, 1996.

1079 Saueressig, G., Crowley, J. N., Bergamaschi, P., Brühl, C., Brenninkmeijer, C. A.  
 1080 M., and Fischer, H.: Carbon 13 and D kinetic isotope effects in the reactions of  $\text{CH}_4$   
 1081 with  $\text{O}(^1\text{D})$  and  $\text{OH}$ : New laboratory measurements and their implications for the  
 1082 isotopic composition of stratospheric methane, *J. Geophys. Res.*, 106, 23127-23138,  
 1083 2001.

1084 Schmitt, J., Seth, B., Bock, M., van der Veen, C., Möller, L., Sapart, C. J.,  
 1085 Prokopiou, M., Sowers, T., Röckmann, T., and Fischer, H.: On the interference of Kr  
 1086 during carbon isotope analysis of methane using continuous-flow combustion-isotope  
 1087 ratio mass spectrometry, *Atmos. Meas. Tech.*, 6, 1425-1445, 2013.

1088 Seibert, P. and Frank, A.: Source-receptor matrix calculation with a Lagrangian  
 1089 particle dispersion model in backward mode, *Atmos. Chem. Phys.*, 4, 51-63, 2004.

1090 Snover, A. K. and Quay, P. D.: Hydrogen and carbon kinetic isotope effects  
 1091 during soil uptake of atmospheric methane, *Global Biogeochem. Cycles*, 14, 25-39,  
 1092 2000.

1093 Spahni, R., Chappellaz, J., Stocker, T. F., Louergue, L., Hausammann, G.,  
 1094 Kawamura, K., Flückiger, J., Schwander, J., Raynaud, D., Masson-Delmotte, V., and  
 1095 Jouzel, J.: Atmospheric Methane and Nitrous Oxide of the Late Pleistocene from  
 1096 Antarctic Ice Cores, *Science*, 310, 1317-1321, DOI: 1310.1126/science.1120132,  
 1097 2005.

1098 Spahni, R., Wania, R., Neef, L., Weele, M. v., Pison, I., Bousquet, P.,  
 1099 Frankenberg, C., Foster, P. N., Joos, F., Prentice, I. C., and Velthoven, P. v.:  
 1100 Constraining global methane emissions and uptake by ecosystems, *Biogeosciences*, 8,  
 1101 1643–1665, doi:1610.5194/bg-1648-1643-2011., 2011.

1102 Sperlich, P., Buizert, C., Jenk, T. M., Sapart, C. J., Prokopiou, M., Rockmann, T.,  
 1103 and Blunier, T.: An automated GC-C-GC-IRMS setup to measure palaeoatmospheric  
 1104  $\delta^{13}\text{C}\text{-CH}_4$ ,  $\delta^{15}\text{N}\text{-N}_2\text{O}$  and  $\delta^{18}\text{O}\text{-N}_2\text{O}$  in one ice core sample, *Atmos Meas Tech*, 6,  
 1105 2027-2041, 2013.

1106 Sperlich, P., Uitslag, N. A. M., Richter, J. M., Rothe, M., Geilmann, H., Veen, C.  
 1107 v., Röckmann, T., Blunier, T., and Brand, W. A.: Development and evaluation of a  
 1108 suite of isotope reference gases for methane in air, submitted to *Atmos. Meas. Tech.*  
 1109 *Disc.*, 2016. 2016.

1110 Stohl, A., Forster, C., Frank, A., Seibert, P., and Wotawa, G.: Technical note: The  
 1111 Lagrangian particle dispersion model FLEXPART version 6.2, *Atmos. Chem. Phys.*,  
 1112 5, 2461-2474, 2005.

1113 Sturm, P., Tuzson, B., Henne, S., and Emmenegger, L.: Tracking isotopic  
 1114 signatures of  $\text{CO}_2$  at the high altitude site Jungfrauoch with laser spectroscopy:  
 1115 analytical improvements and representative results, *Atmos. Meas. Tech.*, 6, 1659-  
 1116 1671, 2013.

1117 Tarasova, O. A., Brenninkmeijer, C. A. M., Assonov, S. S., Elansky, N. F.,  
 1118 Röckmann, T., and Brass, M.: Atmospheric  $\text{CH}_4$  along the Trans-Siberian railroad  
 1119 (TROICA) and river Ob: Source identification using stable isotope analysis, *Atmos.*  
 1120 *Environ.*, 40, 5617-5628, 2006.

1121 Tuzson, B., Henne, S., Brunner, D., Steinbacher, M., Mohn, J., Buchmann, B.,  
 1122 and Emmenegger, L.: Continuous isotopic composition measurements of tropospheric

1123 CO<sub>2</sub> at Jungfraujoch (3580 m a.s.l.), Switzerland: real-time observation of regional  
 1124 pollution events, *Atmos. Chem. Phys.*, 11, 1685-1696, 2011.

1125 Tuzson, B., Mohn, J., Zeeman, M. J., Werner, R. A., Eugster, W., Zahniser, M.  
 1126 S., Nelson, D. D., McManus, J. B., and Emmenegger, L.: High precision and  
 1127 continuous field measurements of  $\delta^{13}\text{C}$  and  $\delta^{18}\text{O}$  in carbon dioxide with a cryogen-  
 1128 free QCLAS, *Appl. Phys. B-Lasers and Optics*, 92, 451-458, 2008.

1129 Umezawa, T., Aoki, S., Nakazawa, T., and Morimoto, S.: A High-precision  
 1130 Measurement System for Carbon and Hydrogen Isotopic Ratios of Atmospheric  
 1131 Methane and Its Application to Air Samples Collected in the Western Pacific Region,  
 1132 *Journal of the Meteorological Society of Japan*, 87, 365-379, 2009.

1133 Umezawa, T., Machida, T., Aoki, S., and Nakazawa, T.: Contributions of natural  
 1134 and anthropogenic sources to atmospheric methane variations over western Siberia  
 1135 estimated from its carbon and hydrogen isotopes, *Global Biogeochem. Cycles*, 26,  
 1136 2012a.

1137 Umezawa, T., Machida, T., Ishijima, K., Matsueda, H., Sawa, Y., Patra, P. K.,  
 1138 Aoki, S., and Nakazawa, T.: Carbon and hydrogen isotopic ratios of atmospheric  
 1139 methane in the upper troposphere over the Western Pacific, *Atmos. Chem. Phys.*, 12,  
 1140 8095-8113, 2012b.

1141 Vermeulen, A. T., Hensen, A., Popa, M. E., van den Bulk, W. C. M., and  
 1142 Jongejan, P. A. C.: Greenhouse gas observations from Cabauw Tall Tower (1992-  
 1143 2010), *Atmos. Meas. Tech.*, 4, 617-644, 2011.

1144 Wächter, H., Mohn, J., Tuzson, B., Emmenegger, L., and Sigrist, M. W.:  
 1145 Determination of N<sub>2</sub>O isotopomers with quantum cascade laser based absorption  
 1146 spectroscopy, *Optics Express*, 16, 9239-9244, 2008.

1147 WMO: 17th WMO/IAEA Meeting on Carbon Dioxide, Other Greenhouse Gases,  
 1148 and Related Measurement Techniques (GGMT-2013) 10-13 June 2013, GAW Report  
 1149 No. 213,, World Meteorological Organization, Geneva, Switzerland, Beijing, China,  
 1150 2014.

1151 Wolf, B., Merbold, L., Decock, C., Tuzson, B., Harris, E., Six, J., Emmenegger,  
 1152 L., and Mohn, J.: First on-line isotopic characterization of N<sub>2</sub>O above intensively  
 1153 managed grassland, *Biogeosciences*, 12, 2517-2531, 2015.

1154 Yamada, K., Ozaki, Y., Nakagawa, F., Tanaka, M., and Yoshida, N.: An  
 1155 improved method for measurement of the hydrogen isotope ratio of atmospheric  
 1156 methane and its application to a Japanese urban atmosphere, *Atmos. Environ.*, 37,  
 1157 1975-1982, 2003.

1158 Zazzeri, G., Lowry, D., Fisher, R. E., France, J. L., Lanoiselle, M., and Nisbet, E.  
 1159 G.: Plume mapping and isotopic characterisation of anthropogenic methane sources,  
 1160 *Atmos. Environ.*, 110, 151-162, 2015.

1161